Semiclassical theory of transport in a random magnetic field

F. Evers and A. D. Mirlin*
Institut für Theorie der Kondensierten Materie, Universität Karlsruhe, 76128 Karlsruhe, Germany

D. G. Polyakov†
Institut für Theorie der Kondensierten Materie, Universität Karlsruhe, 76128 Karlsruhe, Germany
and Institut für Nanotechnologie, Forschungszentrum Karlsruhe, 76021 Karlsruhe, Germany

P. Wölfle
Institut für Theorie der Kondensierten Materie, Universität Karlsruhe, 76128 Karlsruhe, Germany
(Received 8 January 1999)

We present a systematic description of the semiclassical kinetics of two-dimensional fermions in a smoothly varying inhomogeneous magnetic field $B(\mathbf{r})$. The nature of the transport depends crucially on both the strength B_0 of the random component of $B(\mathbf{r})$ and its mean value $\overline{B}$. For $\overline{B}=0$, the governing parameter is $\alpha=d/R_0$, where d is the correlation length of disorder and R_0 is the Larmor radius in the field B_0. While for $\alpha\ll 1$ the Drude theory applies, at $\alpha\gg 1$ most particles drift adiabatically along closed contours and are localized in the adiabatic approximation. The conductivity is then determined by a special class of trajectories, the ''snake states,'' which percolate by scattering at saddle points of $B(\mathbf{r})$ where the adiabaticity of their motion breaks down. The external field $\overline{B}$ also suppresses the diffusion by creating a percolation network of drifting cyclotron orbits. This kind of percolation is due only to a weak violation of the adiabaticity of the cyclotron rotation, yielding an exponentially fast drop of the conductivity at large $\overline{B}$. In the regime $\alpha\gg 1$, the crossover between the snake-state percolation and the percolation of the drift orbits with increasing $\overline{B}$ has the character of a phase transition (localization of the snake states) smeared exponentially weakly by nonadiabatic effects. The *ac* conductivity also reflects the dynamical properties of particles moving on the fractal percolation network. In particular, it has a sharp kink at zero frequency and falls off exponentially at higher frequencies. We also discuss the nature of the quantum magneto-oscillations. Detailed numerical studies confirm the analytical findings. The shape of the magnetoresistivity at $\alpha\sim 1$ is in good agreement with experimental data in the fractional quantum Hall regime near half filling. [S0163-1829(99)01236-9]

I. INTRODUCTION

The transport properties of two-dimensional (2D) particles moving in a spatially random magnetic field (RMF) $\mathbf{B}(\mathbf{r})$ oriented perpendicularly to the plane have attracted considerable interest in the last few years. This interest is largely motivated by the relevance of the problem to the composite-fermion (CF) description[1,2] of a half-filled Landau level. Within this approach, the electron liquid in a strong magnetic field is mapped–by means of a Chern-Simons gauge transformation – to a fermion gas subject to a weak effective magnetic field. Precisely at half filling, the average value of the Chern-Simons gauge field compensates the effect of the external magnetic field. The RMF appears in this model after taking static disorder into account: fluctuations of the local filling factor induced by the random potential of impurities lead to a local mismatch between the gauge and external magnetic fields. A number of observations[3] of Fermi-surface features near half-filling give strong experimental support to the model of the effective magnetic field. Apart from the composite-particle models involving fictitious fields, 2D electron systems with a real RMF can be directly realized in semiconductor heterostructures by attaching to the latter superconducting[4,5] or ferromagnetic[6,7] overlayers.

The peculiarity of transport properties of 2D electrons in a random field $B(\mathbf{r})$ shows up most distinctly in systems with *smooth* inhomogeneities. The case of long-range disorder is most important also experimentally – since the compressible state in a half-filled Landau level is observed in high-mobility samples. In the latter, a large correlation radius of potential fluctuations, d, is determined by a wide ''spacer'' between the electron gas and the doped layer containing ionized impurities. Likewise, inhomogeneities of the RMF created by the ferromagnetic overlayers in[6,7] appear to be fairly long ranged. The large value of the correlation radius d (as compared to the interelectron distance) allows to describe the electron kinetics *quasiclassically*.

It is well known that quantum interference effects may cause localization of noninteracting particles in an infinite 2D system even for arbitrarily weak disorder. This has been shown to be the case for charged particles in a RMF.[8,9] Specifically, the RMF problem belongs to the unitary universality class, with the localization length ξ growing extremely fast with the dimensionless conductance $g=\sigma_{xx}/(e^2/h)$,

$$\xi\propto\exp(\pi^2 g^2). \tag{1}$$

These theoretical results are in full agreement with the recent extensive numerical study.[10] According to Eq. (1), already

 ©1999 The American Physical Society

for $g \gtrsim 1.5$ the localization length is larger than any reasonable system size, and the quasiclassical approach is fully justified.

Let us stress that we consider the situation in which the smooth RMF constitutes the only type of disorder present. This should be contrasted with the starting point of Ref. 11, where the main contribution to the resistivity was assumed to be given by a short-range random scalar potential, while a long-range RMF was considered as a small perturbation.

The purpose of this paper is to examine the transport in a long-range RMF in detail, with particular emphasis on the conductivity in an external (homogeneous) magnetic field $\overline{B} = \langle B(\mathbf{r}) \rangle$ and/or at finite frequency ω. We complement the analytical analysis by numerical simulations. The importance of the latter is due to the fact that in the most interesting part of the parameter space the transport is dominated by the phenomenon of percolation, so that only estimates ''by order of magnitude'' are available at the analytical level.

In Sec. II, we study the dc conductivity in a long-range RMF $\delta B(\mathbf{r})$ at zero $\overline{B}$. The character of the $\overline{B}=0$ transport is determined by the parameter $\alpha = d/R_0$, where $R_0 = v_F(mc/eB_0)$ is the Larmor radius in the field B_0 which is a characteristic amplitude of the fluctuations, v_F the Fermi velocity. At $\alpha \ll 1$, the classical dynamics is of conventional diffusive nature and $\sigma_{xx} \sim (e^2 n d/m v_F)/\alpha^2$, where n is the particle density. At strong disorder ($\alpha \gg 1$), the conductivity is determined by a small *fraction* of classical trajectories – so-called ''snake states''[12,13] – which percolate through the system by winding around the lines of zero $B(\mathbf{r})$ and yield $\sigma_{xx} \sim (e^2 n d/m v_F)/\alpha^{1/2} (\ln \alpha)^{1/4}$. The crossover from the $1/\alpha^2$ to $1/\alpha^{1/2}$ behavior of σ_{xx} at $\alpha \sim 1$ is confirmed by our numerical simulations. Furthermore, the latter allow us to find the numerical value of σ_{xx} for the CF problem (for which $\alpha \simeq 1/\sqrt{2}$ lies in the crossover region).

In Sec. III, we consider the case of strong $\overline{B}$. Increasing $\overline{B}$ also leads to a suppression of the conventional diffusive motion and a transition to a percolation regime, even if $\alpha \ll 1$. The physics of this phenomenon is, however, quite distinct from the snake-state percolation. In the limit of large $\overline{B}$, the dynamics of drifting cyclotron orbits is governed by an adiabatic invariant (magnetic flux through one cyclotron orbit). In the adiabatic approximation, the particles drift along the closed magnetic field contours and hence are localized. It is only a weak *nonadiabatic* scattering between drift trajectories that yields a finite conductivity. This localization effect is similar to the formation of a ''stochastic web''[14,15] in a slowly varying scalar random potential in the presence of an external homogeneous magnetic field. The conductivity due to the weak nonadiabaticity falls off *exponentially* fast at large $\overline{B}$: $\ln \sigma_{xx} = -A(\alpha)(\overline{B}/B_0)^2$, where the coefficient $A(\alpha)$ scales as $\alpha^{4/3}$. Note that the conductivity in the CF problem ($A \sim 1$) falls off *sharply* beyond a *small* deviation from half-filling.

The manner in which the conductivity crosses over into the adiabatic regime is qualitatively different in the cases of weak and strong disorder. At $\alpha \gg 1$ [Sec. III E], the transport regimes controlled by the snake states (weak $\overline{B}$) and by the nonadiabatic dynamics of the cyclotron orbits (strong $\overline{B}$) are separated by a sharp *transition* accompanied by an abrupt change of σ_{xx}. At the critical point, the percolation network formed by the extended snake states falls apart into disconnected clusters, while the nonadiabatic scattering yields only a slight smearing of the critical singularity.

For $\alpha \sim 1$, which is the regime relevant to the CF problem, we perform a numerical simulation to calculate the magnetoresistance $\rho_{xx}(\overline{B})$. The obtained curves are in good agreement with experimental findings: they show a weak positive magnetoresistance at low $\overline{B}$, crossing over to a fall-off of ρ_{xx} with increasing $\overline{B}$. Further, we analyze the quantum oscillations of $\rho_{xx}(\overline{B})$ [Sec. III F] and show that, in contrast to the conventional Shubnikov-de Haas effect in a short-range random potential, they start to develop only when the dimensionless conductivity $\sigma_{xx}/(e^2/h)$ drops down to a value of order of unity.

In Sec. IV, we discuss the transport in the RMF at finite frequency ω. We find strong deviations of the ac conductivity from the Drude behavior, especially in the percolation regime, i.e. when α and/or $\overline{B}$ is large. At small ω, we find a *nonanalytical* ($\propto |\omega|$) contribution to $\sigma_{xx}(\omega)$, which is determined by returns of the particle to the same spatial regions after a time $\sim 1/|\omega|$. At higher frequencies and large $\overline{B}$, the ac conductivity takes the form $\sigma_{xx}(\omega) \propto |\omega|^{3/7}$, since ω itself starts to determine the width of the percolating ''stochastic web'' responsible for the conductivity. At still larger frequencies the *ac* conductivity starts to drop exponentially reflecting the ''ballistic'' motion of drifting orbits (or snake states) on short scales.

Section V summarizes our findings. The analytical results of Secs. II and III were partly presented in the Letter.[16]

II. DC TRANSPORT IN ZERO MEAN MAGNETIC FIELD

We begin by formulating the model to be studied. We consider noninteracting particles in the RMF $\overline{B} + \delta B(\mathbf{r})$ with mean $\overline{B}$ and the correlator $\langle \delta B(0) \delta B(\mathbf{r}) \rangle = B_0^2 f(r)$, where $f(0)=1$. We assume that the function $f(r)$ is characterized by a single spatial scale, which is the correlation length of the RMF. In particular, in the CF model with the electron density n equal to the charged impurity density n_i we have $B_0 = (\hbar c/e)(k_F/\sqrt{2}d)$ and $f(r) = (1 + r^2/4d^2)^{-3/2}$, where $k_F^2 = 4\pi n$ (note that the electron gas is fully spin polarized near $\nu = 1/2$; we discard the spin degree of freedom throughout the paper). In this section we confine ourselves to the case of zero $\overline{B}$. The RMF with zero mean is characterized by two length scales: d and the cyclotron radius R_0 in the field B_0. Defining the parameter $\alpha = d/R_0$, we can distinguish the weak-RMF regime $\alpha \ll 1$, where the mean-free path $l \gg R_0 \gg d$, and the regime of strong fluctuations $\alpha \gg 1$, where one should expect drastic deviations from the Drude picture. We will explore these two limiting cases analytically. However, since the value of α corresponding to the CF problem lies in the crossover region, we will turn to numerical simulations in order to get σ_{xx} of the CF's.

A. Weak disorder

We start with the simple case of $\alpha \ll 1$. In this limit, the CF trajectories are only slightly bent on the scale of d, so that

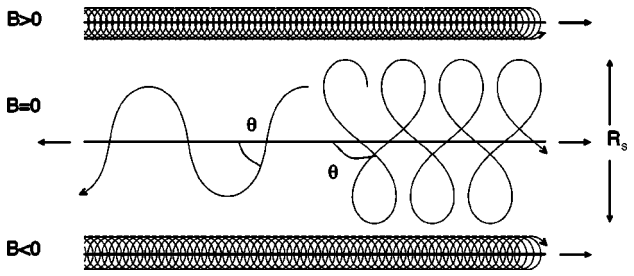

FIG. 1. Types of trajectories in a strong random magnetic field: drifting orbits along nonzero B contours and snake states near $B=0$ lines. Geometry of a snake state is characterized by the angle θ $(0<\theta<\pi)$ at which the trajectory crosses the zero-field contour. Note that the direction of motion of the snake state with $\theta<\theta_c$ (left) is opposite to that for $\theta>\theta_c$ (right), where $\theta_c\simeq 131°$. The width R_s of the bundle of snake state trajectories is also indicated.

the Born approximation is valid. Accordingly, for the transport scattering time one gets[2,17] $\tau_{tr}^{-1}=v_F^{-1}(eB_0/mc)^2\int_0^\infty dr f(r)=2\alpha^2 v_F/d$, where the CF effective mass $m=\hbar k_F/v_F$ is introduced. The Drude conductivity at zero $\overline{B}$, $\sigma_{xx}=e^2 n\tau_{tr}/m$, then reads

$$\sigma_{xx}=\frac{e^2}{h}\frac{k_F d}{4\alpha^2},\quad \alpha\ll 1. \tag{2}$$

B. Dynamics of the snake states

Let us now turn to the strong-RMF regime, $\alpha\gg 1$, keeping $\overline{B}=0$. The seemingly innocent assumption about the chaotic character of the particle dynamics, which enabled us to represent the conductivity in the form $e^2 n\tau_{tr}/m$, is not valid anymore. Most particles are now out of play since they are caught in cyclotron orbits drifting along the closed lines of constant $B(\mathbf{r})$ (''van Alfvén drift''). In the adiabatic limit, their drift trajectories are periodic and so do not contribute to the conductivity. Still, however large B_0 is, there are classical paths, which are not localized and percolate through the system by meandering around the lines of zero $B(\mathbf{r})$. The conductivity is determined by the particles that move along these extended ''snake states''[12] (Fig. 1).

Note that there is only one single percolating path on the manifold of the $B(\mathbf{r})=0$ contours; yet, the conductivity is nonzero since the snake-state trajectories form a bundle of finite width, $R_s\sim d/\alpha^{1/2}$ (see Fig. 1). The conducting network is made up of those snake states that can cross over from one critical zero-B line to another. This coupling of two adjacent percolating clusters occurs near the critical saddle points of $B(\mathbf{r})$, which are nodes of the transport network. The crucial role of the saddle points is that they break down the adiabaticity of the snake-state dynamics, as we are going to explain below.

Everywhere except in small regions near the saddle points, the motion along the rapidly oscillating snake-state trajectories around the zero-B contours conserves the adiabatic invariant (see also Ref. 13)

$$I_\perp=m\oint \dot{y}dy. \tag{3}$$

Here, y and $\dot{y}$ are the distance and the velocity in the direction perpendicular to the zero-B line, and the integral is taken over one period of the oscillations. The conservation of the quantity $I_\perp$ can be established directly by considering the evolution of the angle $\theta(x)$ the snake-state trajectory forms with the line of zero field $(y=0)$ at position x along this line as a consequence of the smoothly varying gradient $b(x)=|\partial B(x,y)/\partial y|_{y=0}$. The adiabatic invariant is parametrized as

$$I_\perp(b,\theta)=4mv_F^{3/2}(2mc/eb)^{1/2}F(\theta), \tag{4}$$

where $F(\theta)$ is a dimensionless function of order unity which can be found explicitly:

$$F(\theta)=(1-\cos\theta)\int_0^1 d\xi\sqrt{(1-\xi^4)+\cos\theta(1-\xi^2)^2}. \tag{5}$$

Note that $I_\perp(b,\theta)$ may be written also as $(e/c)\Phi(b,\theta)$, where Φ is the magnetic flux through the area encircled by the snake-state trajectory and the zero-B line in one oscillation period. We represent the equation $dI_\perp/dx=0$ in the form of a scaling relation for the snake-state angle

$$\frac{d\theta}{d\ln b}=G(\theta),\quad G^{-1}(\theta)=2\frac{d}{d\theta}\ln F(\theta). \tag{6}$$

This equation expresses the adiabatic invariance in terms of the fact that, given boundary conditions [$\theta(x_0)$ and $b(x_0)$ at some point x_0], the angle θ at a point x of the trajectory is completely determined by the gradient $b(x)$ at the same point. Equation (5) gives the asymptotic expressions for $G(\theta)$

$$G(\theta)\simeq\frac{\theta}{4},\quad \theta\to 0; \tag{7}$$

$$G(\theta)\simeq-\frac{2}{3}\frac{1}{(\pi-\theta)\ln\dfrac{1}{\pi-\theta}},\quad \theta\to\pi. \tag{8}$$

Equations (6) and (7) tell us that $\theta(x)$ obeys the scaling

$$\frac{\theta(x_1)}{\theta(x_2)}=\left[\frac{b(x_1)}{b(x_2)}\right]^{1/4} \tag{9}$$

in the limit of small harmonic oscillations $\theta\to 0$. The singularity of $G(\theta)$ in the opposite limit of $\theta\to\pi$ is a precursor of the bifurcation, which accompanies the break away of the trajectory from the zero-B line at $\theta=\pi$ (see Fig. 2, top). The functions $F(\theta)$ and $G(\theta)$ in the whole range of θ are shown in Figs. 3(a) and 3(b).

The remarkable point to notice is that $G(\theta)$ changes sign at some $\theta=\theta_c$ (which is $\simeq 131°$). More specifically, $G(\theta)$ behaves singularly around θ_c, as $(\theta-\theta_c)^{-1}$, which corresponds to a maximum in $F(\theta)$ at this point. This behavior of $I_\perp(\theta)$ means that the velocity of the snake states $v_s(\theta)$ (which is the average of $\dot{x}$ over one period) must change sign at $\theta=\theta_c$, i.e., the snake state is ''reflected'' at the point x_c defined by the equation $\theta(x_c)=\theta_c$ (Fig. 2, bottom). Indeed, as follows from Eq. (4), the constancy of $I_\perp[\theta(x)]$ cannot be maintained on *both* sides of the point x_c. Note also that, in

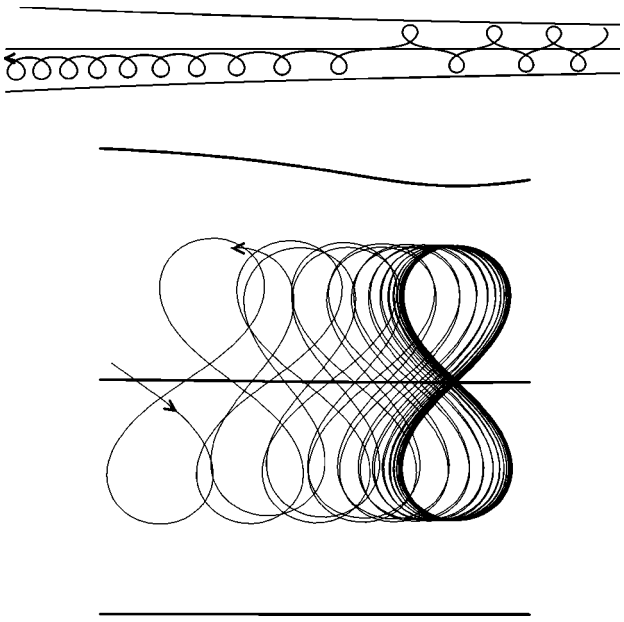

FIG. 2. ''Serpentology.'' Top: transformation of a snake state with large θ into a drifting orbit with decreasing gradient of the magnetic field; bottom: reflection of a snake state by a magnetic bottle-neck.

terms of the time evolution of θ, the change in sign of the function $G(\theta)$ at $\theta=\theta_c$ means that the time derivative $\dot{\theta}$ retains the sign it had before the reflection. In fact, one can show, by solving the problem with constant gradient b exactly, that

$$v_s(\theta)=v_F F'(\theta)\frac{1+\frac{1}{2}\cos^2\theta}{\frac{3}{2}\sin\theta F(\theta)+\cos\theta F'(\theta)}, \qquad (10)$$

i.e., $v_s(\theta)$ interpolates between $v_s(0)=v_F$ and $v_s(\pi)=-v_F$ and vanishes at $\theta=\theta_c$ [see Fig. 3(c)]. It is worth noting that the period of the oscillations $T_s(\theta)$ increases monotonically with growing θ

$$T_s(\theta)=\frac{1}{mv_F^2}\left(\frac{3}{2}+\cot\theta\frac{\partial}{\partial\theta}\right)I_\perp(b,\theta), \qquad (11)$$

i.e., $T_s(\theta)$ is equal to $2\pi(mc/ebv_F)^{1/2}$ at $\theta=0$ and diverges as $4(mc/ebv_F)^{1/2}\ln[1/(\pi-\theta)]$ at $\theta\to\pi$. The ''wavelength'' of the snake states along the direction of propagation obviously reads $\Delta x=|v_s|T_s$, while the amplitude of the oscillations in the perpendicular direction is given by $\Delta y=2v_F(mc/ebv_F)^{1/2}\sin(\theta/2)$.

C. Snake-state percolation

The adiabatic nature of the snake-state dynamics means that a typical trajectory is ''trapped'' between two return points x_+ and x_- with $\theta(x_\pm)=\theta_c$ [Fig. 4(a)]. Within the adiabatic picture, the drift motion in such a trap is periodic in time, as demonstrated in Fig. 4(b). Hence, unless nonadiabatic corrections are taken into account, these trajectories do not contribute to the dc conductivity. The nonadiabatic corrections for a typical trajectory with a slowly varying $\theta(x)$ are exponentially weak, so that the motion remains finite on an exponentially long time scale. Yet, this does *not* mean

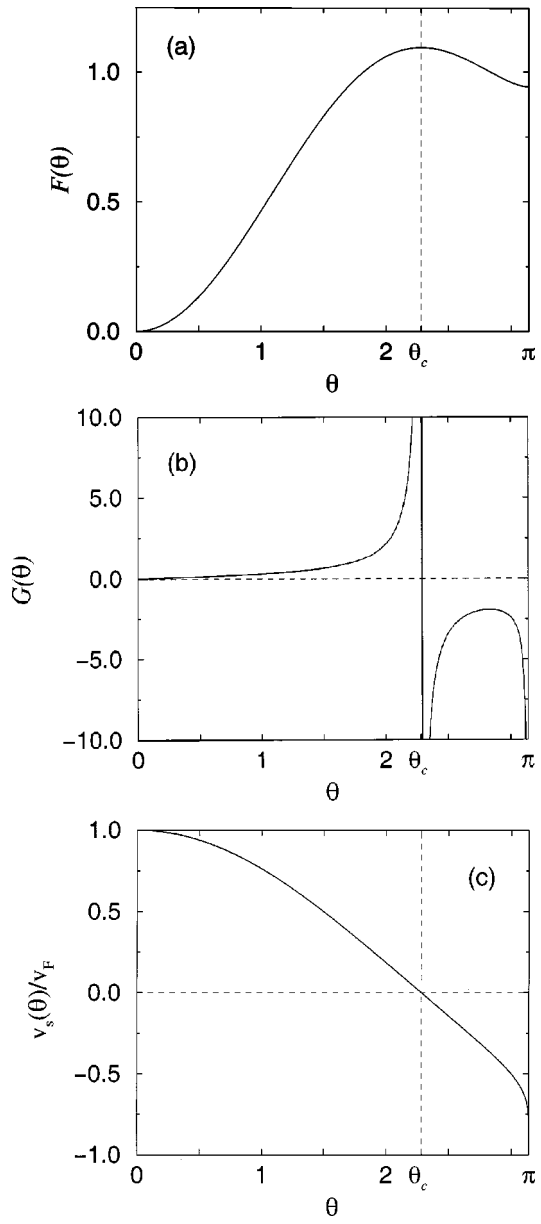

FIG. 3. The functions $F(\theta)$ and $G(\theta)$ determining the adiabatic dynamics of the snake states according to Eqs. (4)–(6), and the snake state velocity $v_s(\theta)$.

that $\sigma_{xx}(\alpha)$ is exponentially suppressed in the limit of large α. The point is that there are rare (but not exponentially rare) places along the zero-B contours where the adiabatic picture fails *completely*. These are regions where the contours pass near the saddle points of $B(\mathbf{r})$.

Consider a snake state that is incident on a saddle point with the impact parameter ρ (Fig. 5). This means that the magnetic field at the saddle point is $B_{\rm sp}\sim B_0\rho/d$ and the distance $R_{\rm min}$ at which the zero-B contour passes the saddle point is $R_{\rm min}\sim\sqrt{d\rho}$. At the saddle point, there is an intersection of two lines of constant $B(\mathbf{r})=B_{\rm sp}$, while two zero-B lines, along which the snake states can propagate, come within the distance $2R_{\rm min}$ from each other. Clearly, if $R_{\rm min}$ is small enough, the snake state can change the zero-field contour. The angle θ, which characterizes the type of the snake-state trajectory, is then also changed, i.e., the adiabaticity

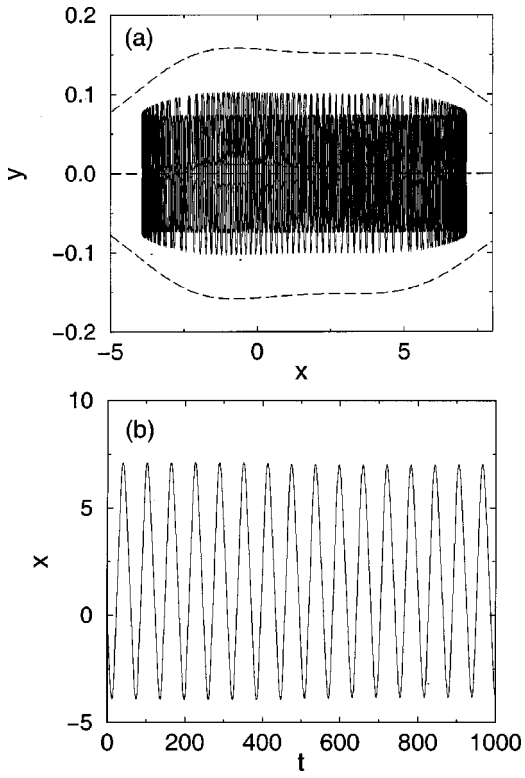

FIG. 4. Snake state in a trap. (a) Real-space trajectory of a particle trapped between two bottle-necks. The scales of the x and y axes differ by a factor $\simeq 25$: the figure is ''compressed'' in the x-direction. The dashed lines show the contours of the constant magnetic field. (b) Time evolution of the x coordinate. It is seen that the drift motion in the trap is almost periodic.

will be broken down upon ''scattering'' on the saddle point. To understand the parameters, consider first the case of $\rho = 0$ (''direct hit''). The snake state propagates then along a straight line with decreasing gradient $b(x) \sim B_0 x/d$, where x is measured from the saddle point. According to Eq. (9), $\theta(x) \propto x^{1/4}$ decreases when the particle approaches the saddle point, while, as follows from Eq. (11), the wavelength Δx diverges as $x^{-1/2}$. The adiabatic picture is valid only as long as $\Delta x(x)$ is much smaller than the scale on which the magnetic field changes, i.e., $\Delta x(x) \ll x$ near the saddle point,

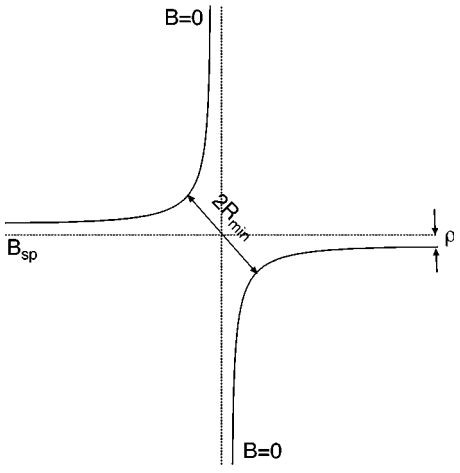

FIG. 5. Geometry of a saddle point.

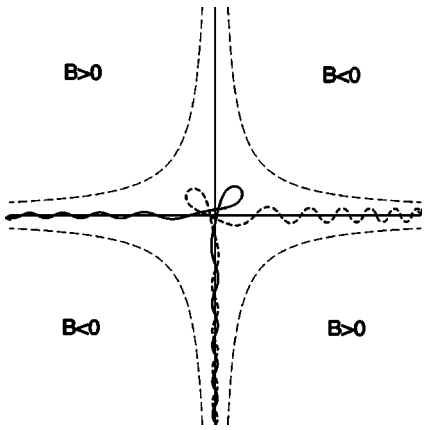

FIG. 6. Scattering of a snake state at a saddle point. The particle may turn either left or right, depending on the initial conditions.

which gives the condition $x \gg x_c$, where x_c is the characteristic wavelength of the ''last'' oscillation before the particle hits the saddle point. For typical trajectories with $\theta \sim 1$ and $\Delta x \sim (dR_0)^{1/2}$ at $x \sim d$, this condition fails at $x \lesssim x_c \sim d/\alpha^{1/3}$. Now, as is clear from Fig. 6, whether the particle will be scattered to the left of the saddle point or to the right is determined by the initial phase of the snake-state oscillations. This sensitivity to the phase signals the breakdown of the adiabaticity.

We now turn to the case of finite ρ. At large enough ρ, the typical snake-state trajectory does not change the zero-B line: the condition is that the angle $\theta(x_c)$, with which the trajectory comes to the saddle point, be much smaller than the ratio $R_{\min}/x_c$. Substituting $\theta(x_c) \sim (x_c/d)^{1/4}$ [see Eq. (9)], we get $\rho \gg d/\alpha^{5/6}$. However, the adiabatic invariance is broken at the saddle point in a wider range of ρ: the condition for the curvature of the zero-B line to be large on the scale of the wavelength is $R_{\min} \lesssim x_c$, which gives $\rho \lesssim \rho_s$, where

$$\rho_s \sim d/\alpha^{2/3}. \tag{12}$$

Within this range, the angle θ after the scattering, θ_{out}, is typically of order unity even though the particle is incident on the saddle point with a small θ (moreover, θ_{out} depends strongly on the phase of the oscillations of the incoming trajectory). As we argue below, the breakdown of the adiabatic invariance at $\rho \lesssim \rho_s$ results in the randomization of the incident snake states over the outgoing links.

Now consider how the particles propagate between such nonadiabatic saddle points. The saddle points with $\rho \lesssim \rho_s$ are distributed sparsely along the zero-B trajectories with the linear density $\sim \rho_s/d^2$. Therefore, only a small fraction of the snake states can escape the adiabatic traps on their way between two such saddle points: most trajectories are localized in between. The snake state is not trapped if $\theta(x) < \theta_c$ everywhere on its trajectory between the collisions with the saddle points. According to Eq. (9), this is possible for trajectories with sufficiently small θ. Indeed, consider a snake state, which has a small angle $\theta \ll 1$ in a typical place with the gradient $b \sim B_0/d$. Typically, it will be able to travel a long distance, by far larger than d, until its angle reaches the value θ_c: this will occur in a fluctuation of the magnetic field with the anomalously high gradient $b \sim B_0/d\theta^4$. Since the

probability $p(b)$ that the gradient at a given point exceeds some value b is determined by the Gaussian statistics, $p(b) = \exp(-b^2/\langle b^2\rangle)$, we find that the state will typically run ballistically the distance $L(\theta)$ obeying the equation $L(\theta)p(B_0/d\theta^4)/d \sim 1$, which gives $L(\theta) \sim d\exp(\theta^{-8})$. Hence, using $L(\theta_s)/d \sim d/\rho_s \sim \alpha^{2/3}$, we conclude that the states with the angles $\theta \ll \theta_s$, where

$$\theta_s \sim (\ln \alpha)^{-1/8}, \tag{13}$$

will typically get through to the saddle point.

We, thus, conclude that the particles with $\theta \lesssim \theta_s$ propagate between saddle points ''ballistically'' with the longitudinal velocity $v_s \simeq v_F$, while others are simply out of play. Now we turn to construct the overall picture of the snake-state propagation. The scattering on a saddle point is actually a multistep process. The fact that the angle $\theta_{\rm out}$ is typically ~ 1 means that, having collided with a saddle point once, the particle almost inevitably returns back to it with a new angle of incidence θ': in effect, the trajectory ''sticks'' to the saddle point. However, after many mappings $\theta \to \theta_{\rm out} \to \theta'$, the multiple reflections establish a stochastic distribution of the angle $\theta_{\rm out}$ characterizing the outgoing trajectory. Also, after many attempts the particle will go to the left or to the right with equal probability. This randomization of $\theta_{\rm out}$ and of the direction of motion is clearly seen in the numerical simulation in Ref. 13. Once the particle picks up the angle $\theta_{\rm out} \sim \theta_s/\alpha^{1/12}$, it will move ballistically until it reaches the next saddle point. Here, the factor $\alpha^{-1/12}$ is related to the fact that the angle $\theta(x)$ will increase $\propto x^{1/4}$ on the scale of d, so that the particle must have $\theta_{\rm out}$, which is $(x_c/d)^{1/4}$ times smaller than θ_s. At the new saddle point the whole process will repeat itself. Since the saddle points are separated by the large distance $\sim d^2/\rho_s$, the average time it takes the particle to move to the next saddle point is determined by the ballistic propagation between them, which requires the time $t_b \sim d^2/\rho_s v_F \sim (d/v_F)\alpha^{2/3}$, not by the multiple attempts to ''break away'' with large $\theta_{\rm out}$, which end in returns to the starting point. Indeed, assuming the full randomization of $\theta_{\rm out}$, we estimate the number of such attempts, until the particle picks up the angle $\theta_{\rm out} \lesssim \theta_{\rm out}^{(c)} = \alpha^{-1/12}(\ln\alpha)^{-1/8}$ necessary to reach the next saddle-point, as $N \sim 1/\theta_{\rm out}^{(c)}$. According to what is said above, the initial condition $\theta_{\rm out}$ allows the particle to advance the distance

$$L(\theta_{\rm out}) \sim d \times \begin{cases} \alpha^{-1/3}\theta_{\rm out}^{-4}, & \theta_{\rm out} \gtrsim \alpha^{-1/12} \\ \exp[(\alpha^{1/12}\theta_{\rm out})^{-8}], & \theta_{\rm out} \lesssim \alpha^{-1/12}. \end{cases} \tag{14}$$

Therefore, the average ''waiting time'' the particle spends in the unsuccessful attempts to reach the next saddle point is

$$t_w \sim N \int_{\theta_{\rm out}^{(c)}} d\theta_{\rm out} L(\theta_{\rm out})/v_F \sim (d/v_F)\alpha^{2/3}/\ln\alpha. \tag{15}$$

Thus, the total time it takes to get through from one saddle point to another is indeed determined by $t_b \gg t_w$.

D. Conductivity in a strong random magnetic field

Now let us calculate the conductivity at $\alpha \gg 1$. As was mentioned at the very beginning, most trajectories do not contribute to σ_{xx} since they follow periodic drift orbits. Next, we turned to consider a special class of the trajectories – the snake states. However, as we showed above, most snake states are also localized in the adiabatic traps and only those with angles smaller than θ_s can propagate along the lines of zero B. At this point, we have to be concerned about the topology of the zero-B contours. The first thing to notice is that all the contours are closed except one and this one percolating contour by itself cannot yield a finite conductivity. The conductivity is nonetheless finite since the snake states in fact form a conducting *network* of finite width. The nodes of the network are *critical* saddle points, where two adjacent percolating contours come close to each other. Note that most of the saddle points that the particle hits on its way between the critical ones only connect up small closed loops and so do not create a connected network. This happens only at the critical saddle points, where the snake states can cross over from one critical zero-B line of length $L_s \sim \alpha^{14/9}d$ to another. We use here the results of the percolation theory (for a review see, e.g., Ref. 18): $L_s \sim d(d/\rho_s)^{\nu+1}$, where $\nu = 4/3$ is the critical exponent that controls the size of the critical cluster $\xi_s \sim d(d/\rho_s)^{\nu}$, so that the ratio of the length of the trajectory and the distance from the starting point $L_s/\xi_s \sim d/\rho_s$. The characteristic distance between the nodes, i.e., the size of the elementary cell ξ_s, is then $d\alpha^{8/9}$. On length scales longer than ξ_s, the particle dynamics can be viewed as fully stochastic. We estimate the macroscopic diffusion coefficient as $D \sim \nu_s D_s$, where $\nu_s \sim L_s R_s \theta_s^2/\xi_s^2$ is the fraction of particles residing in the delocalized snake-states and $D_s \sim \xi_s^2 \times v_F/L_s$ is their diffusion coefficient. Note that ν_s contains a factor θ_s^2 – since the density of the snake states is determined in the phase space parametrized by both the angle θ and real-space coordinate: accordingly, one factor θ_s comes from the calculation of the fraction of the plane covered by the conducting snake states, while the other describes their fraction in the θ space. We, thus, have $D \sim v_F R_s \theta_s^2$ and, correspondingly,[19]

$$\sigma_{xx} \sim \frac{e^2}{h}\frac{k_F d}{\alpha^{1/2}\mathcal{L}}, \quad \mathcal{L} \sim \ln^{1/4}\alpha, \quad \alpha \gtrsim 1. \tag{16}$$

It is worth noting that the percolation *enhances* the conductivity: by comparison with the Born approximation [Eq. (2)], the conductivity is $\sim \alpha^{3/2}/\mathcal{L}$ times larger (though the localization effects are strong and naively one might have expected the opposite). Let us also note that σ_{xx} given by Eq. (16) is larger by a factor of $\sim \alpha^{1/2}/\mathcal{L}$ than that obtained for $\alpha \gg 1$ in Ref. 20 by using an ''eikonal approach.'' The fault in Ref. 20 is not with the quasiclassical approximation itself, but with the method of disorder averaging, which neglects the localization of particles and the percolating character of the transport through the snake states.

We now turn to the numerical simulation. To calculate the conductivity tensor components $\sigma_{\mu\nu}$ we evaluate numerically the classical current response function,

$$\sigma_{\mu\nu} = e^2\rho_F \int_0^\infty dt \langle v_\mu(0) v_\nu(t)\rangle, \tag{17}$$

where $\rho_F = m/2\pi\hbar^2$ is the density of states and the average is taken over the disorder realizations and starting points of the trajectory. Typically, evaluation of the conductivities in-

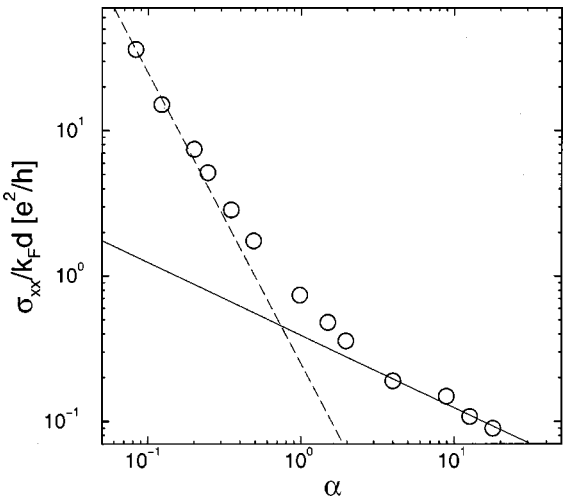

FIG. 7. dc conductivity at $\overline{B}=0$, as a function of the parameter α. The dashed and the full lines correspond to the theoretical asymptotics (2) and (16), respectively. Statistical errors do not exceed the symbol size.

volved averaging over $\sim 10^3 \div 10^4$ trajectories. The numerical results for σ_{xx} in Fig. 7 fully confirm the analytical findings above. For small α, the results are in good agreement with the Born approximation formula, Eq. (2), while at $\alpha \sim 1$ a crossover to the $\alpha^{-1/2}$ behavior, Eq. (16), takes place. At $\alpha = 1/\sqrt{2}$ (the value relevant to the CF problem at $n = n_i$ and in the absence of impurity correlations) we find $\sigma_{xx} \simeq 1.0(e^2/h)k_F d$, which is a factor of ~ 2 larger than the Born approximation value. This improves the agreement with the experimentally found CF conductivity (defined as the inverse of the measured resistivity at $\nu = 1/2$), though the typical experimental values of σ_{xx} are still larger than the one we obtain by a factor of $\sim 2-3$. This remaining discrepancy might be attributed to correlations in the distribution of the charged donors,[21] which reduces the effective strength of the random potential and thus reduces α. The resistivity data in zero external magnetic field (as contrasted to zero effective magnetic field acting on CF's) indeed indicate that the model of statistically independent impurity positions overestimates the amount of disorder.[22,21] It is also worth noting here, in view of the controversy about the effective mass of the CF's,[2,23–25] that in the RMF model σ_{xx} at zero $\overline{B}$ [Eqs. (2) and (16)] does not depend on m (neglecting the corrections[26] related to the interaction between the CF's).

III. DC TRANSPORT IN NONZERO MEAN MAGNETIC FIELD

We now consider the conductivity at finite $\overline{B}$. Let us first discuss the case of $\alpha \sim 1$, when the conductivity $\sigma(\overline{B})$ can be parameterized as a function of the *single* variable $\overline{B}/B_0$. As shown in the previous section, at small $\overline{B}/B_0$ we are at the crossover between the uncorrelated diffusion and the snake-state percolation. Now, at $\overline{B} \gg B_0$ the particle dynamics is a slow van Alfvén drift of the cyclotron orbits along the lines of constant $\delta B(\mathbf{r})$. It follows that the conductivity is determined by a percolation network of trajectories close to the $\delta B(\mathbf{r}) = 0$ lines. From the point of view of topology of the network, the situation is thus similar to that at zero $\overline{B}$ and $\alpha \gg 1$. What is crucially different, however, is the mechanism of the percolation. Specifically, at large $\overline{B}$ there is no stochastic mixing at the nodes of the percolation network: unlike the snake states at $\overline{B}=0$, the rapidly rotating cyclotron orbits pass unharmed through the critical saddle points of $\delta B(\mathbf{r})$ without crossing over to the adjacent cell. In the high-$\overline{B}$ limit, the mixing occurs on the links of the network and is only due to the weak scattering between the drift trajectories.

In order to calculate the conductivity at $\overline{B} \gg B_0$, we should integrate out the fast cyclotron rotation, taking care not to lose the effect of the nonadiabatic mixing. Specifically, we have to go beyond the standard separation of the fast and slow degrees of freedom, known as the drift approximation. The parameter that governs this separation is δ/d, where δ is a characteristic shift of the guiding center after one cyclotron revolution. The drift approximation is represented as a power series in $\delta/d \ll 1$. In our problem at $\alpha \sim 1$, this parameter is the ratio $B_0/\overline{B}$. Therefore, if $\overline{B} \gg B_0$, the adiabatic description is good on *microscopic* scales. The key point, however, is that the conductivity is strictly zero at the level of the drift approximation – since the drift orbits are periodic in the thermodynamic limit. The effects that break the adiabatic invariance and lead to the transitions between the drift orbits are *exponentially* weak at $\delta/d \ll 1$.

A. Single-impurity scattering

The problem of the scattering between the drift trajectories in the static RMF,[16] as well as a similar problem for a random scalar potential, considered recently in Ref. 14, is a particular example of the broad class of problems dealing with nonconservation of an adiabatic invariant. Despite the general interest of this problem, any systematic expansion capable of giving the scattering rate *beyond* the exponential accuracy, has proven to be a tough exercise. To consider a transparent example, we formulated and solved parametrically exactly a *single*-scattering problem.[27] Specifically, we introduce a weak homogeneous gradient $\boldsymbol{\epsilon}$ of the background magnetic field and consider the interaction with an ''impurity'' modeled by a spatially localized perturbation $\delta B(\mathbf{r})$ of size d, so that the total field

$$B(\mathbf{r}) = \overline{B}[1 + \boldsymbol{\epsilon}(y/R_c)] + \delta B(\mathbf{r}), \tag{18}$$

where R_c is the cyclotron radius in the field $\overline{B}$. The guiding center coordinate y averaged over the cyclotron orbit, $\rho = \langle y \rangle_c$, plays the role of an impact parameter. The particle entering the system at $x = -\infty$ with $\langle y \rangle_c = \rho_i$ will leave it at $x = \infty$ along the trajectory with $\langle y \rangle_c = \rho_i + \Delta\rho$, where $\Delta\rho$ is the nonadiabatic shift we are interested in. In this single-impurity scattering problem, the shift is a perfectly well-defined quantity. To first order in δB, the exact solution is given by

$$\Delta\rho = \gamma I, \quad I = \int_{-\infty}^{\infty} dt \, \frac{\delta B[\mathbf{r}_0(t)]}{\overline{B}} y_0(t). \tag{19}$$

Here, $\mathbf{r}_0(t)$ is the unperturbed trajectory for $\delta B = 0$,

$$\gamma(\epsilon)=\omega_c\left\langle \dot{y}_0(t)\int_0^t dt'\dot{x}_0(t')/\dot{y}_0^2(t')\right\rangle_c , \qquad (20)$$

$\omega_c=e\bar{B}/mc$, and the angular brackets denote averaging over one cyclotron period. In the limit $\epsilon\to 0$ the constant $\gamma\to -1$. We can further simplify the model by assuming that δB is a function of x only. In this case, the integral in Eq. (19) is evaluated at $\epsilon\ll 1$ by the saddle-point method to give

$$\Delta\rho=-\frac{2v_F}{\bar{B}}\sqrt{\frac{\epsilon}{\pi}}\cos\left(\frac{2}{\epsilon}-\frac{\pi}{4}\right)\cos\varphi_0 \times\int_{-\infty}^{\infty}dt\cos\omega_c t\,\delta B\left(\frac{\epsilon}{2}v_F t-R_c\right). \qquad (21)$$

This formula expresses the nonadiabatic shift in terms of the asymptotics of the Fourier transform of the smooth function $\delta B(x)$ – thus demonstrating explicitly the exponential smallness of $\Delta\rho$. It shows that the parameter that governs the exponential falloff of $\Delta\rho$ is $d/\delta\gg 1$, where $\delta=\pi\epsilon R_c$, while the ratio d/R_c may be arbitrary. Note that the pre-exponential factor happens to oscillate wildly as $\epsilon\to 0$. These oscillations are geometric resonances due to the commensurability of two length scales R_c and δ. Remarkably, the series of the resonances is defined by the properties of the unperturbed solution (''self-commensurability'') and not by the shape of the scatterer. This means that the oscillations are damped with increasing strength of the perturbation[27] – since the resonance condition cannot be met simultaneously everywhere on a strongly perturbed trajectory. Another peculiar feature of the nonadiabatic shift is its sensitivity to the phase φ_0 of the cyclotron rotation of the incident electron ($\Delta\rho\propto\cos\varphi_0$).

In the CF problem, a charged impurity located at a distance d from the plane occupied by the electron gas creates the axially symmetric perturbation $\delta B(\mathbf{r})=\delta B_0 d^3(r^2+d^2)^{-3/2}$. Because of the branch points at $r=\pm id$ in this expression, the integrand in Eq. (19) will contain the exponentially small factor $\exp[-(2\omega_c/\epsilon v_F)\sqrt{[y_0(t)-\rho_i]^2+d^2}]$. The lengthy general result reduces to

$$\Delta\rho\simeq 8\pi d\frac{\delta B_0}{\bar{B}}\frac{\sqrt{R_c d}}{\delta}\cos\varphi_0\cos\left(\frac{2}{\epsilon}-\frac{\pi}{4}\right)\exp\left(-\frac{2\pi d}{\delta}\right) \qquad (22)$$

at $\rho_i=0$ in the limit $d\gg R_c$. Equation (22) reflects the features of the nonadiabatic shift discussed above: the exponential smallness, the oscillations with changing ϵ, and the oscillatory dependence on the phase φ_0. These results were confirmed by numerical simulations in Ref. 27. Note that Eq. (22) implies that the drift trajectory is only slightly perturbed by $\delta B(\mathbf{r})$.

B. Optimum fluctuation

In the transport problem one has to average over an ensemble of impurities. What is crucial for the averaging process is that the drift velocity is itself determined by the fluctuations of the impurity field. The nonlinear problem gets, therefore, much more involved as compared to the single-scattering model above, but the principal features of the nonadiabatic scattering remain unchanged and the main message can be simply stated: Because of the exponentially strong dependence of the shift on the parameters of the single scatterer, the conductivity is determined by *rare* places with an anomalously high rate of nonadiabatic transitions.[14,16] Accordingly, one can neglect correlations between consecutive transitions from one drift orbit to another and each nonadiabatic shift can be considered independently. Since the nonadiabatic scattering rate increases as the drift motion gets faster, the effective scatterers, sparsely distributed along the percolating trajectories, are characterized by anomalously sharp changes of the RMF. The problem now is to find the density and the parameters of these scatterers.

The nonadiabatic shift $\Delta\rho=\Delta\rho_x+i\Delta\rho_y$ (in complex notation) after one scattering reads

$$\Delta\rho=v_F\int dt e^{i\omega_c t+i\varphi_0}A(t), \qquad (23)$$

where the smooth function $A(t)$ varies slowly on the scale of ω_c^{-1} and is given by the following average taken over one cyclotron period:

$$A(t)=\langle e^{i\chi(t)}\rangle_c , \quad \chi(t)=\frac{e}{mc}\int_0^t dt'\,\delta B[\mathbf{r}(t')]. \qquad (24)$$

The integral that determines the random phase $\chi(t)$ should be done on the exact trajectory $\mathbf{r}(t)$. Note that Eq. (23) gives the nonadiabatic shift both along and across the drift trajectory. Since only the latter is of interest, one should project the result of the integration (23) onto the axis perpendicular to the direction of the drift of the outgoing particle.

Since the nonadiabatic mixing is determined by the short wavelength Fourier harmonics of the perturbation [Eq. (23)], it is the analytical properties of the function $A(t)$ and, therefore, of the correlator $\langle\delta B(0)\delta B(\mathbf{r})\rangle$ that are important. In the CF problem, this correlator has branch points as a function of r at $r=\pm 2id$. However, in order to calculate the scattering probability, which is given by Eq. (23), one has to find the singularities in $\delta B[\mathbf{r}(t)]$ as a function of *time* t and average the result. For a given perturbation $\delta B(\mathbf{r})$ this purely mechanical problem of finding the Fourier asymptotics of the integral along the path $\mathbf{r}(t)$ may be quite complex, but we can circumvent the difficulties by performing the configurational averaging first. As was already mentioned, the effective scatterers are characterized by anomalously large fluctuations of the drift velocity

$$v_d(s)=v_F(R_c/2B)|\nabla B(s)|, \qquad (25)$$

where s is the coordinate along the path. To see this, one can use the exact solution of the single-scattering problem considered above. Let us first assume, for the purpose of illustration, that the large $v_d(s)$ does not change appreciably on the scale of d. Equation (22) then tells us that a single impurity located on the trajectory that passes through the fluctuation with large v_d yields $\Delta\rho(v_d)\propto\exp(-d\omega_c/v_d)$. One sees that $\Delta\rho(v_d)$ grows exponentially with increasing v_d. Now, the linear density of the fluctuations with large v_d along the percolating path is of order $p(v_d)$, where the Gaussian probability that the drift velocity at a given point is larger than v_d reads

$$p(v_d)=\exp(-v_d^2/2\langle v_{dx}^2\rangle);$$

$$\langle v_{dx}^2\rangle=\frac{3}{16}v_F^2\left(\frac{R_c}{d}\right)^2\left(\frac{B_0}{\overline{B}}\right)^2. \tag{26}$$

Averaging $[\Delta\rho(v_d)]^2$ with $p(v_d)$, we thus get

$$\langle[\Delta\rho(v_d)]^2\rangle\propto\exp(-S_{\min});\qquad S_{\min}=3\left(\frac{d^2\omega_c^2}{2\langle v_{dx}^2\rangle}\right)^{1/3}.$$

The ''optimum'' drift velocity that determines this average is $v_d^0=\langle v_{dx}^2\rangle^{1/2}(4d^2\omega_c^2/\langle v_{dx}^2\rangle)^{1/6}$. As is clear, $v_d^0\gg\langle v_{dx}^2\rangle^{1/2}$ at $\overline{B}\gg B_0$. The optimum fluctuations yield the Gaussian behavior of the scattering rate:

$$S_{\min}=c(\overline{B}/B_0)^2,\quad \overline{B}/B_0\gg 1, \tag{27}$$

with the coefficient $c=18^{1/3}\simeq 2.62$ (here we assumed $\alpha=1/\sqrt{2}$). This simple derivation of the exponential dependence of $\langle[\Delta\rho(v_d)]^2\rangle$ captures the essential physics and yields a correct parametric estimate for $S_{\min}$; however, it is not exact in that $v_d(s)$ in the optimum fluctuation is not, in fact, constant on the scale of d, and for this reason it does not give the correct value of the numerical coefficient c in Eq. (27). To obtain the asymptotically exact numerical coefficient in $S_{\min}$, we have to use the optimum-fluctuation method in the whole configurational space. The optimum configuration is characterized by the function $v_d(s)$ and the shape of the drift trajectory. We write the phase factor $e^{i\omega_c t}$ in Eq. (23) as $e^{i\varphi(s)}$, where we introduce the s dependent phase

$$\varphi(s)=\omega_c\int_0^s\frac{ds'}{v_d(s')}, \tag{28}$$

and notice that the exponent $S_{\min}$ is determined by the phase $\varphi(s)$ picked up at the singular point of the perturbation $\delta B[\mathbf{r}(t)]$ regarded as a function of the longitudinal coordinate s. As can be verified by varying the shape of the trajectory, the minimum ''action'' $S_{\min}$ is acquired along a straight path and the quantity to be calculated is therefore

$$S_{\min}=-\ln\left\langle\exp\left[i\omega_c\int_{-id}^{id}\frac{ds}{v_d(s)}\right]\right\rangle, \tag{29}$$

where the integral should be done along the straight line connecting the points $s=-id$ and $s=id$ in the complex plane of the variable s.[28] This average determines, with exponential accuracy, the diffusion coefficient $D_\perp\propto\exp(-S_{\min})$, which is defined as

$$D_\perp=\lim_{t\to\infty}t^{-1}\langle[\Delta\rho(t)]^2\rangle, \tag{30}$$

where $\Delta\rho(t)$ is the nonadiabatic shift across the percolating drift trajectory in time t. The exponent can be written as a sum of two terms, $S_{\min}=W_1+W_2$, where

$$W_1=\frac{1}{2}\int\frac{d^2\mathbf{q}}{(2\pi)^2}v_{dx\mathbf{q}}^0\Gamma_{\mathbf{q}}^{-1}v_{dx-\mathbf{q}}^0 \tag{31}$$

$$W_2=i\omega_c\int_{-id}^{id}\frac{dx}{v_{dx}^0(x,0)},$$

and

$$\Gamma_{\mathbf{q}}=\langle v_{dx}v_{dx}\rangle_{\mathbf{q}}=\left(\frac{hc^2mv_F^2}{e^2\overline{B}^2}\right)^2nq_y^2e^{-2qd} \tag{32}$$

is the Fourier transform of the drift-velocity correlation function $\Gamma(\mathbf{r})=\langle v_{dx}(0)v_{dx}(\mathbf{r})\rangle$. Here, W_1 determines the probability for the optimum fluctuation $v_{dx}^0(\mathbf{r})$ to occur, while W_2 describes the nonadiabatic scattering on this fluctuation. The variational equation $\delta W/\delta v_{dx}^0=0$ yields

$$v_{dx}^0(\mathbf{r})=i\omega_c\int_{-id}^{id}\frac{dx'}{[v_{dx}^0(x',0)]^2}\Gamma(x-x',y), \tag{33}$$

which is a nonlinear integral equation for $v_{dx}^0(x,0)$ with $x\in(-id,id)$. Its solution defines, by means of analytical continuation, the optimum fluctuation on the real axis of x. Dimensional analysis of this equation shows that the solution has the form $v_{dx}^0(\mathbf{r})=v_F(B_0/\overline{B})\mathcal{G}(\mathbf{r}/d)$, where $\mathcal{G}$ is a dimensionless function of order unity, which leads again to Eq. (27). To find the exact value of c, one has to determine the function $\mathcal{G}$, which requires solving the integral equation (33). We used a variational approach, choosing the trial function $v_{dx}^0(\mathbf{r})=\kappa\Gamma(\mathbf{r})$ with the variational parameter κ. This trial function is the optimal fluctuation for the (slightly different) problem of finding a large value $v_{dx}^0(0)$ at the point $\mathbf{r}=0$ and should give a good estimate for c. The result is $c\simeq 2.28$, close to the value found above within the simplified consideration neglecting the spatial variation of v_{dx} on the scale of d.

C. Magnetotransport at $\alpha\sim 1$: Conductivity of the composite fermions at $\nu\neq 1/2$

We are now prepared to calculate the conductivity at $\overline{B}\gg B_0$. Similarly to the case of the snake-state percolation, the nonadiabatic transitions create a conducting network with the elementary cell of size $\xi\sim d(d/R_d)^{4/3}$ and perimeter $L\sim\xi d/R_d$, where R_d, the width of the links of the network composed of the drift trajectories, obeys the equation

$$R_d^2\sim D_\perp L/v_d. \tag{34}$$

This equation is the condition of connectivity of the network. The conductivity due to the nonadiabatic mixing of the drift trajectories is thus given by

$$\sigma_{xx}\sim\frac{me^2}{\hbar^2}v_dR_d\propto\frac{e^2}{h}k_Fd\exp\left(-\frac{3}{13}S_{\min}\right). \tag{35}$$

The dissipative transport is seen to be strongly suppressed beyond the scale $\overline{B}\sim B_0$.[29] Let us emphasize that the crossover to the adiabatic regime occurs in the CF system at a small deviation from half-filling $\nu=1/2$: $\overline{B}\sim B_0$ corresponds to the shift $|\nu-1/2|\sim 1/k_Fd\ll 1$.

Calculation of the conductivity tensor components at $\overline{B}\lesssim B_0$ cannot be done analytically at $\alpha\sim 1$. We have per-

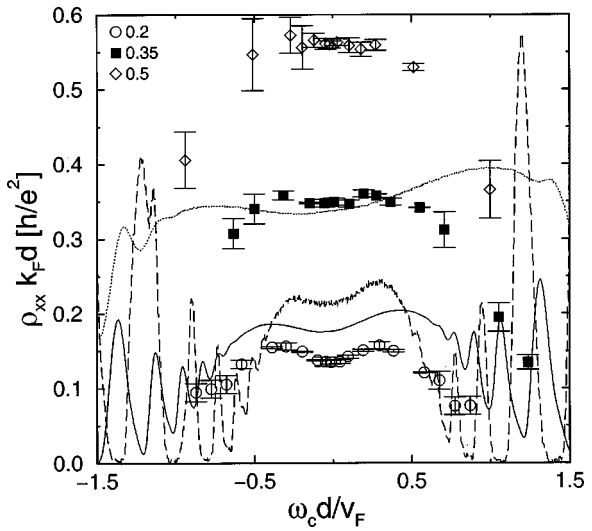

FIG. 8. Magnetoresistivity at $\alpha=0.2$, 0.35, and 0.5; the cyclotron frequency in the scaling of the x axis refers to the external magnetic field, $\omega_c=e\overline{B}/mc$. The full, dashed, and dotted lines show the experimental magnetoresistivity around $\nu=1/2$ according to the data of Refs. 30, 31, and 25, respectively (in this case ω_c refers to the effective magnetic field $\overline{B}=B-2hcn/e$). The sample parameters (carrier density n, undoped spacer width d and zero-field mobility μ) are $n=1.53\times10^{11}\,\mathrm{cm}^{-2}$, $d=80$ nm, $\mu=5\times10^6\,\mathrm{cm}^2/\mathrm{V\,s}$, (Ref. 30), $n=0.86\times10^{11}\,\mathrm{cm}^{-2}$, $d=80$ nm, $\mu=10.5\times10^6\,\mathrm{cm}^2/\mathrm{V\,s}$ (Ref. 31), $n=1.31\times10^{11}\,\mathrm{cm}^{-2}$, $d=120$ nm, $\mu=3.5\times10^6\,\mathrm{cm}^2/\mathrm{V\,s}$ (Ref. 25).

formed extensive numerical simulations to study the overall shape of the magnetoresistivity. The results for $\alpha=0.2$, 0.35, and 0.5 are shown in Fig. 8, in comparison with experimental data on the magnetoresistivity in the vicinity of $\nu=1/2$ from Refs. 25, 30, and 31. We recall, that although a simple model of uncorrelated impurities with the concentration $n_i=n$ gives $\alpha=1/\sqrt{2}$, the actual value of α may be somewhat smaller because of impurity correlations. As is seen, the experimental curves are reasonably close to the numerical data with $\alpha\sim0.25\div0.35$. The numerical results show a positive magnetoresistance at $\overline{B}\lesssim B_0$, which is followed at larger $\overline{B}$ by a falloff in agreement with the analytical prediction (27). Both these features are clearly observed in the experiment. Better agreement between the theory and the experiment is hardly possible, taking into account the difference between the experimental data obtained by different groups and on different (though nominally very close) samples. Sufficiently far from half-filling the experimental curves start to show magnetooscillations, which have not been included in the classical model above. We will discuss the issue of the magnetooscillations below.

D. Magnetotransport at weak disorder, $\alpha\ll1$

We now turn to consider the case of weak disorder $\alpha\ll1$. The Gaussian behavior of the conductivity at large $\overline{B}$ is in fact a general property of the nonadiabatic transport in the RMF. We can use the same optimum fluctuation method as for the CF system above to get

$$S_{\min}=c(2\alpha^2)^{2/3}(\overline{B}/B_0)^2,\quad \overline{B}/B_0\gg\alpha^{-1}. \tag{36}$$

This result is valid if $\overline{B}$ is large enough; namely, it requires that the shift of the guiding center in the field of the optimum fluctuation after one cyclotron revolution, δ, and the Larmor radius R_c be both smaller than d. The condition $R_c\ll d$ breaks down with decreasing $\overline{B}$ at $\overline{B}/B_0\sim\alpha^{-1}$. Provided $\alpha\ll1$, the exponent (36) taken at the crossover point is large, which means that $\delta\ll d$ and we are still deep in the adiabatic regime. Next we consider the regime $\overline{B}/B_0<\alpha^{-1}$. What changes at smaller $\overline{B}$ is that the drift velocity of the guiding center at point $\mathbf{r}$ is now determined by an effective RMF $\delta B^{\mathrm{eff}}(\mathbf{r})$, the amplitude of which is smaller than B_0 because of the averaging of the fluctuations over the large cyclotron radius. We define $\delta B^{\mathrm{eff}}(\mathbf{r})$ by writing the general expression for the drift velocity to first order in $\delta B/\overline{B}$ in the form

$$\mathbf{v}_d(\mathbf{r})=-\frac{e}{mc}\int_0^{2\pi}\frac{d\varphi}{2\pi}[\,\delta\mathbf{B}(\mathbf{r}+\mathbf{R}_\varphi)\times\mathbf{R}_\varphi] \tag{37}$$

$$=v_F\frac{R_c}{2\overline{B}^2}[\nabla\,\delta B^{\mathrm{eff}}(\mathbf{r})\times\overline{\mathbf{B}}],$$

where $\mathbf{R}_\varphi=R_c(\cos\varphi,\sin\varphi)$ and φ is the phase of the cyclotron rotation around the point $\mathbf{r}$. Stokes' theorem then yields

$$\delta B^{\mathrm{eff}}(\mathbf{r})=\frac{1}{\pi R_c^2}\int_{R\leqslant R_c}d^2\mathbf{R}\,\delta B(\mathbf{r}+\mathbf{R}). \tag{38}$$

Equation (38) tells us that δB^{eff} is given by the magnetic flux through the cyclotron orbit, so that the drift occurs along the lines of constant *flux* (not the lines of constant magnetic field averaged along the orbit). If $\delta B(\mathbf{r})$ is a smoothly varying function on the scale of R_c, $\delta B^{\mathrm{eff}}(\mathbf{r})$ coincides with $\delta B(\mathbf{r})$, otherwise the averaging leads to a strong suppression of the fluctuations of $\delta B^{\mathrm{eff}}(\mathbf{r})$. More specifically, at $R_c\gg d$ the field $\delta B^{\mathrm{eff}}(\mathbf{r})$ is characterized by two spatial scales: it has a short-range component whose correlation radius remains of order d – its characteristic amplitude is

$$B_0^{\mathrm{eff}}\sim B_0(d/R_c)^{3/2} \tag{39}$$

– and a long-range component which has a larger amplitude $\sim B_0 d/R_c$ but fluctuates on the much longer scale of R_c. Since the drift velocity is given by the gradient of $\delta B^{\mathrm{eff}}(\mathbf{r})$, it is the short-range fluctuations that determine $\mathbf{v}_d(\mathbf{r})$. Applying the optimum fluctuation method, we now have

$$S_{\min}\sim\alpha^{1/3}\overline{B}/B_0,\quad \alpha^{-1/3}\lesssim\overline{B}/B_0\lesssim\alpha^{-1}. \tag{40}$$

At $\overline{B}/B_0\sim\alpha^{-1/3}$ the factor $e^{-S_{\min}}$ becomes of order unity and at smaller $\overline{B}$ the adiabatic invariance does not hold anymore.

Let us briefly discuss the deviations from the Drude behavior at low-magnetic fields $\overline{B}$ in the case of weak disorder ($\alpha\ll1$). The Drude theory predicts zero magnetoresistance, $\Delta\rho_{xx}/\rho_{xx}=0$. Bending of the cyclotron trajectories on the scale of d leads to a small negative contribution to the magnetoresistance:[16,20]

$$\frac{\Delta\rho_{xx}}{\rho_{xx}}=-\frac{3}{2}\alpha^2\left(\frac{\overline{B}}{B_0}\right)^2\ln\min\left\{\frac{1}{\alpha^2},\frac{B_0}{\alpha\overline{B}}\right\}. \tag{41}$$

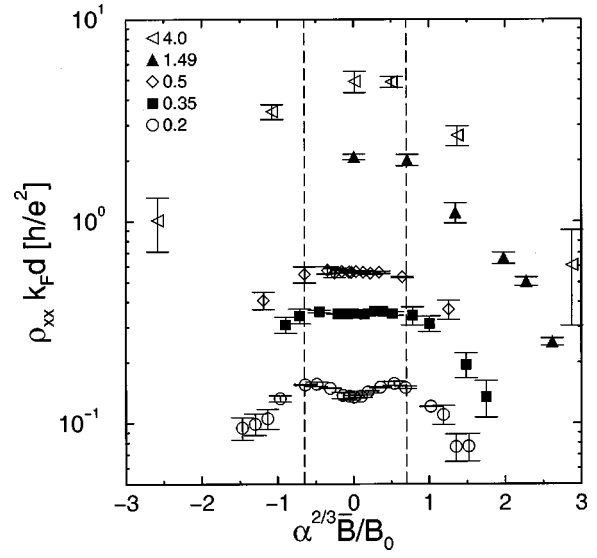

FIG. 9. Magnetoresistivity at $\alpha=0.2$, 0.35, 0.5, 1.5, and 4. The dashed lines show the critical field B_c, at which the exponential falloff begins for $\alpha \gtrsim 1$; see Eq. (42).

However, our numerical results demonstrate a pronounced positive magnetoresistance in the range $\bar{B}/B_0 \lesssim \alpha^{-1/3}$, so that the resistivity shows a maximum at $\bar{B}/B_0 \sim \alpha^{-1/3}$ before it starts to drop exponentially according to Eqs. (35), (36), and (40). This positive magnetoresistance remains for all α below ~ 0.5, see Figs. 8 and 9, and is strikingly similar to the experimentally observed positive magnetoresistance of composite fermions near $\nu=1/2$. A detailed theoretical analysis of this positive magnetoresistance (which is determined by returns of a particle to a vicinity of the starting point) will be given elsewhere.[32]

E. Magnetotransport at strong disorder, $\alpha \gg 1$: Localization of the snake states at $\bar{B} > \bar{B}_c$

Let us address now the finite-$\bar{B}$ transport in the opposite limit of strong disorder $\alpha \gg 1$. The asymptotics (36) remains unmodified at sufficiently large $\bar{B}$, namely, at $\bar{B} \gg B_0/\alpha^{1/2}$, where $R_c \ll R_s$. At smaller $\bar{B}$, the trajectories close to the zero-δB lines become localized in the adiabatic traps [Sec. II] and start to transform into the snake states. A new feature is thus the appearance of a competing mechanism of the conduction – the snake-state percolation. Indeed, the snake-state trajectories are tied to the lines of $B(\mathbf{r})=0$, where $B(\mathbf{r})=\bar{B}+\delta B(\mathbf{r})$ is the *total* field. On the other hand, the percolating trajectories are those that follow the lines of $\delta B(\mathbf{r})=0$, independent of $\bar{B}$. At large $\bar{B} \gg B_0/\alpha^{1/2}$, the percolating and snake-state trajectories are therefore separated in space: the snake states are closed orbits localized deep inside the elementary cells of the conducting network. Now, at $\bar{B} \lesssim B_0/\alpha^{1/2}$, the nonadiabatic scattering is due to two mechanisms: the exponentially weak nonadiabatic corrections to the dynamics of the snake-state angle θ and the breakdown of the adiabaticity of the snake states at the saddle points. The latter mechanism leads to the formation of percolation clusters. Thus, there exists a well-defined value of $\bar{B}=\bar{B}_c$ below which the snake states form a continuous network and can percolate through the entire system. The critical field $\bar{B}_c$ is of the order of $B_0\rho_s/d$, i.e.,

$$\bar{B}_c \sim B_0 \alpha^{-2/3}, \tag{42}$$

which is the characteristic amplitude of the magnetic field at the critical saddle points. It is worth stressing that there is a clear separation of the adiabatic and snake-state regimes: the nonadiabatic scattering within the finite clusters only leads to an exponentially narrow uncertainty in the position of the critical point. If one neglects this nonadiabatic smearing of the transition, the conductivity can be expressed as

$$\sigma_{xx} = \frac{e^2}{h}\frac{k_F d}{\alpha^{1/2}\mathcal{L}}\mathcal{F}\left(\frac{\bar{B}}{\bar{B}_c}\right), \tag{43}$$

where $\mathcal{F}(x)$ is a dimensionless function, such that $\mathcal{F}(0)\sim 1$ and $\mathcal{F}(x \geqslant 1)=0$, and σ_{xx} at zero $\bar{B}$ coincides with that in Eq. (16). The magnetoresistivity for $\alpha=1.5$ and $\alpha=4$ is shown on a logarithmic scale in Fig. 9 (for completeness, we also included the data for smaller values of α, which have been already displayed in Fig. 8). We see that the resistivity indeed shows an exponential falloff beyond a characteristic field consistent with Eq. (42).

To find the critical behavior of $\sigma_{xx} \propto (\bar{B}_c - \bar{B})^t$ near $\bar{B}_c$, we formulate an auxiliary percolation problem in more conventional terms. Consider equipotential contours in a random potential with a characteristic amplitude V_0 and the correlation length d and pick up all contours within the energy band $(-\Delta,\Delta)$, where $\Delta \ll V_0$. These contours form a percolation network, the size of the elementary cell of which is $\xi(\Delta) \sim d(V_0/\Delta)^{4/3}$. The characteristic width of the links of the network is of order $d\Delta/V_0$. This is a standard percolation problem. Now, let us shift the energy band corresponding to the percolation network: namely, we introduce a parameter ε and consider all contours within the band $(-\Delta+\varepsilon, \Delta+\varepsilon)$. Clearly, the system undergoes a percolation transition at $\varepsilon = \pm\Delta$. In this new percolation problem, the length $\xi(\Delta)$ plays a role of the elementary scale, so that the characteristic radius of the percolation cluster is now

$$\xi(\Delta,\varepsilon) \sim \xi(\Delta,0)(\Delta/|\Delta-\varepsilon|)^{4/3}$$

(for positive ε). Next, let particles propagate along the equipotential contours ''ballistically.'' As we know already from Secs. II and III, the conductivity σ of such a network scales as the typical width of the conducting links $d(\Delta-\varepsilon)/V_0$, i.e., $\sigma \propto (\Delta-\varepsilon)$. Assuming that our original problem can be mapped onto the problem above, we will get the critical exponent for the conductivity of the snake-state network $t=1$, i.e., $\mathcal{F}(x)\sim 1-x$ at $x \to 1$.

F. Magneto-oscillations

Until now, we have dealt with the transport properties of *classical* particles. The classical description is justified by the large value of the parameter $k_F d \gg 1$: first, this parameter enabled us to calculate the conductivity by examining the microscopic dynamics in terms of classical *trajectories*; second, it guaranteed the existence of a wide range of the fields

B_0 and $\bar{B}$ in which the thus-calculated conductivity $\sigma_{xx} \gg e^2/h$ [cf. Eqs. (2) and (16)]. It is the latter condition that allowed us to neglect the quantum interference of multiply scattered waves and related localization effects. In this section, we discuss the small quantum oscillations of σ_{xx} as a function of $\bar{B}$, which are conventionally termed the Shubnikov-de Haas (SdH) effect. We argue that the physical picture of the magneto-oscillations in the smooth RMF (and, in fact, in the limit of a long ranged random potential as well) is rather peculiar from the conventional point of view.

We first recall the standard results for the case of a random scalar potential with a sufficiently short correlation length. Within the usual approach,[33,34] the magnetooscillations of σ_{xx} are related to those of the total density of states ρ_F: $\sigma_{xx}^{\rm osc}/\sigma_{xx} \propto \rho_F^{\rm osc}/\rho_F$, where $\sigma_{xx}^{\rm osc}$ and $\rho_F^{\rm osc}$ denote the oscillating parts of σ_{xx} and ρ_F. The damping of the oscillations in low fields is described in terms of the single-particle relaxation time τ_s (also termed sometimes the quantum relaxation time),[35–38,17] which is equal to the transport mean-free time τ_{tr} for the white-noise random potential and is $\sim \tau_{tr}/(k_F d)^2$ for the random potential with correlation length $d \gtrsim k_F^{-1}$. Specifically, the exponent of the Dingle factor $\exp(-S_{\rm SdH})$ is $S_{\rm SdH} = \pi/\omega_c \tau_s$, so that at $\omega_c \tau_s \sim 1$ the oscillations of both the density of states at the Fermi level and the conductivity become strong. We note that this crossover to the strong oscillations occurs in the case of short-range disorder at $\sigma_{xx}/(e^2/h) \sim k_F l (\tau_s/\tau_{tr})^2 \gg 1$, assuming that the ratio τ_{tr}/τ_s is not too large. With further increasing $\bar{B}$, at $\omega_c \tau_s \gg 1$, the density of states exhibits a series of peaks, well separated from each other, so that in the centers of the valleys between the peaks the quantum localization starts to develop rapidly, which leads in turn to the appearance of quantum plateaus in the Hall conductivity. The full Hall quantization takes place, however, at much larger $\bar{B}$, when the value of the conductivity in the center of the peak drops to a value $\sim e^2/h$. Therefore, in the short-range random potential, there exists a parametrically broad region between the appearance of the SdH oscillations and the fully developed quantum Hall effect.

In the case of a white-noise RMF the situation is different. The short-range fluctuations of the magnetic field are accompanied by long-range fluctuations of the random vector-potential. As a result, the single-particle relaxation rate now diverges due to the strong small-angle scattering.[8,17] The divergence is cut off by the characteristic length scale in the problem, which is the cyclotron radius. As a consequence, the damping factor $S_{\rm SdH}$ takes a different form, $S_{\rm SdH} = 4\pi E_F/\omega_c^2 \tau_{tr} = 4\pi \sigma_{xx}/(e^2/h)$.[17] It follows that at $S_{\rm SdH} \sim 1$, where the oscillations become observable, $\sigma_{xx} \sim e^2/h$. This is, therefore, a marginal case: the SdH oscillations become appreciable in the same region of $\bar{B}$ where the quantum localization effects get strong.

Now, let us consider the limit of the long-range RMF. In this case, the oscillations of the total density of states are damped exponentially strongly in the whole region where the classical conductivity is $\gtrsim e^2/h$, and are thus of no importance. However, the crucial thing to notice is that the oscillations of σ_{xx} and of the total density of states ρ_F are no longer directly related to each other. Indeed, as shown above, σ_{xx} is determined with growing $\bar{B}$ by a progressively smaller fraction of the total number of trajectories. In the adiabatic limit, only trajectories close to the zero-δB contours contribute to σ_{xx}. It follows that the oscillations of σ_{xx} are associated with the oscillations of the density of these conducting states *only*. In particular, this means that the SdH effect and the magnetooscillations of thermodynamic quantities (de Haas-van Alfvén effect) will be characterized by completely different damping factors.

We now turn to the Dingle factor for σ_{xx}. Quite generally, the SdH effect is due to the quantum interference of two waves propagating along quasiclassical trajectories for which the number of cyclotron revolutions is different by $\pm N$ for the Nth harmonic of the oscillations.[39,40,17] The Dingle factor for the first (and most prominent) harmonic with $N=1$ can therefore be represented as

$$\exp(-S_{\rm SdH})\cos\psi = \left\langle \sum_\alpha G_\alpha \cos\Phi_\alpha \right\rangle, \qquad (44)$$

where α labels trajectories in a given realization of disorder, G_α is the weight with which the trajectory α contributes to σ_{xx}, $\Sigma_\alpha G_\alpha = 1$, Φ_α is the phase that is acquired by a particle moving along the trajectory after one cyclotron revolution, ψ is the phase of the SdH oscillations, and $\langle\ \rangle$ denotes ensemble averaging. In general, the phase factor $\cos\Phi$ should be averaged both over *different* trajectories and along *one* trajectory. However, in the limit of smooth disorder, the action Φ_α, which is the dimensionless magnetic flux through the cyclotron orbit, is the adiabatic *invariant* characterizing the trajectory. A subtle point here is that the van Alfvén drift occurs along the lines of constant flux Φ – not the lines of constant field B [see Eq. (38)]. At first glance, this difference might seem to be irrelevant in the case of long-range RMF with $d \gg R_c$. In fact, however, it is of crucial importance for the calculation of the amplitude of the oscillations. Let us illustrate this point by first deriving S along the following line of argument. We know already that the extended trajectories form a percolating network along the contours of zero $\delta B(\mathbf{r})$. Since the width of the links of the conducting network is much smaller (in fact, as shown above, exponentially smaller) than R_c, it is a good approximation to place the guiding center on the contour of zero $\delta B(\mathbf{r})$, calculate the RMF flux $\delta\Phi$ through the cyclotron orbit, and average $e^{i\,\delta\Phi}$ over different positions of the guiding center on the zero-δB line. This would give a contribution to the Dingle-factor exponent $S_{\rm SdH} = \langle(\delta\Phi)^2\rangle/2 \sim (eB_0/\hbar c)^2 (R_c^2/d)^4$.[16] In fact, however, the actual trajectory of the guiding center is slightly shifted from the contour of zero $\delta B(\mathbf{r})$ – by an amount that exactly cancels the above contribution to $S_{\rm SdH}$ – since it is the flux that is the adiabatic invariant. It follows that the average over the flux should be done only over *different* trajectories: Φ_α in Eq. (44) is, in the adiabatic limit, constant for a given α.

Having established the conservation of the flux Φ_α along the trajectory we can rewrite Eq. (44) in the following form

$$\exp(-S_{\rm SdH})\cos\psi = \int d\Phi\, G(\Phi)\cos\Phi, \qquad (45)$$

where $G(\Phi)=\langle\Sigma_\alpha G_\alpha\delta(\Phi-\Phi_\alpha)\rangle$ is understood as the ensemble average taken *across* a link of the conducting network. The function $g(\Phi)$ is represented as a narrow peak of width $\Delta\Phi$ centered at $\Phi_0=2\pi(mv_F^2/2\hbar\omega_c)$. The dimensionless magnetic flux $\Delta\Phi$ can be expressed in terms of the width R_d [Eq. (34)] of the link of the conducting network by $\Delta\Phi\sim(e/\hbar c)\Delta B R_c^2$, where $\Delta B\sim B_0 R_d/d$ is the characteristic change of the RMF across the link. We, thus, see that the broadening $\Delta\Phi$ is related to the conductivity of the network [Eq. (35)] and obeys the equation

$$\sigma_{xx}\sim\frac{e^2}{h}\Delta\Phi. \tag{46}$$

This rather remarkable result implies that the Dingle factor e^{-S} is a function of the single variable $g=\sigma_{xx}/(e^2/h)$:

$$\exp[-S_{\mathrm{SdH}}(g)]=\int_{-\infty}^{\infty}dx Q(x)\cos(2\pi g x). \tag{47}$$

Here, we have expressed $G(\Phi)=(2\pi g)^{-1}Q[(\Phi-\Phi_0)/2\pi g]$ in terms of the parameterless function $Q(x)$, which falls off at $|x|\sim 1$ and is normalized according to $\int dx Q(x)=1$. According to Eq. (47), the Dingle factor is represented as the Fourier transform of the smooth function $Q(x)$. It is worth noting that Eq. (47) can be interpreted also in terms of the local Landau levels. In the language of the quasiclassical quantization, the contribution G_N of the Nth Landau level to the conductivity $\sigma_{xx}=\Sigma_N G_N$ falls off beyond the band of width $\Delta N\sim g\gg 1$ around $N=mv_F^2/2\hbar\omega_c$, where the number of effectively conducting Landau levels is determined by the change of the flux across the link, $\Delta N=\Delta\Phi/2\pi$. Represented in terms of ΔN, Eq. (46) takes the familiar form: the conductivity is of the order of e^2/h times the number of the conducting channels in the effective network. Applying Poisson's formula to the sum $\Sigma_N G_N$ we again arrive at Eq. (47).

Hence, the SdH oscillations due to the oscillations of the density of states of the ''conducting'' particles become observable at $g\sim 1$. However, as has been already mentioned, there exists another effect that leads to the appearance of the magnetooscillations: the quantum localization. According to the scaling theory of the quantum Hall effect,[41]

$$S_{\mathrm{QHE}}(g)=2\pi g,\quad g\gg 1, \tag{48}$$

irrespective of any microscopic details, in particular, the value of α. Equations (47) and (48) tell us that both types of oscillations become observable at $g\sim 1$. To decide which oscillations are stronger, one should calculate the Fourier asymptotics (47). This requires knowing the precise shape of the function $Q(x)$. It appears that in the case of the percolation network $Q(x)$ can be obtained only by means of a numerical simulation. Here, we restrict ourselves to concluding that the number of oscillations observed scales in the CF problem as $p_c\sim k_F d/\ln^{1/2}(k_F d)$. Since

$$g\propto k_F d\exp[-(p_c/p)^2],$$

where $p=E_F/\hbar\omega_c$, the oscillations disappear extremely fast with increasing p (i.e., decreasing $\overline{B}$). These findings are in agreement with experimental observations. The typical number of oscillations observed in the best samples with $k_F d\sim 15$ is $p_c=7-9$. The oscillations start indeed to develop at $g\simeq 1$, as shown in Fig. 10, where the experimental data of Ref. 25 are represented in terms of the CF conductivity. Finally, the damping of oscillations with decreasing $\overline{B}$ is extremely fast, so that the Dingle plot is strongly nonlinear.[24,25]

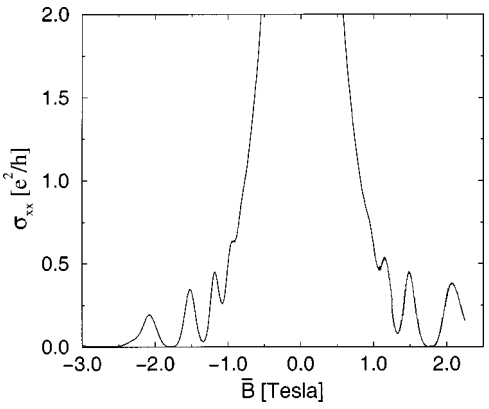

FIG. 10. Composite-fermion conductivity σ_{xx} as a function of the effective magnetic field extracted from the data of Ref. 25. The magneto-oscillations start to develop when the conductivity (in units of e^2/h) drops down to a value ~ 1.

To summarize, in contrast to the text-book example of a short-range potential, the damping of the magnetooscillations in a smooth RMF has the form $\ln\sigma_{xx}^{\mathrm{osc}}\simeq -S(g)$; i.e., the Dingle factor is a function of the dimensionless conductivity only [here $S(g)=\min\{S_{\mathrm{SdH}},S_{\mathrm{QHE}}\}$]. The explicit form of the function $S(g)$ warrants further study.

IV. AC TRANSPORT

The frequency-dependent dissipative conductivity involves the Fourier transform of the retarded velocity-velocity correlator: $\sigma_{xx}(\omega)=e^2\rho_F\langle|v_x|_\omega^2\rangle$, where

$$\langle|v_x|_\omega^2\rangle=\mathrm{Re}\int_0^\infty dt e^{i\omega t}\langle v_x(0)v_x(t)\rangle. \tag{49}$$

In the quasiclassical limit, which we consider here, the integral over t is understood as the integral along a classical trajectory, characterized by the velocity $\mathbf{v}(t)$, while $\langle\ \rangle$ denotes the averaging over the trajectories. The average is taken over all trajectories of electrons at the Fermi level. However, as discussed above, if the magnetic field, either $\overline{B}$ or B_0, is strong enough, most trajectories do not make a significant contribution to the dc conductivity and the transport is governed by the percolation of a small portion of their total number. In this section, we turn to the ac conductivity. We will show that changing the frequency, one effectively probes the motion on the percolating network on different spatial scales. This results in a strong non-Drude frequency dispersion of the conductivity.

A. ac conductivity at $\alpha\sim 1$, $\overline{B}\gg B_0$: application to the composite fermions around $\nu=1/2$

We start with the ac conductivity at $\alpha\sim 1$ in a strong external field $\overline{B}\gg B_0$ (which is relevant to the CF problem at

sufficiently strong deviation from $\nu=1/2$, $\Delta\nu \gg 1/k_F d$). Our analysis in Sec. III relies on the characterization of the electron dynamics at $\overline{B} \gg B_0$ by three degrees of freedom with different frequency scales: the fast cyclotron rotation, the slow drift, and the still slower nonadiabatic diffusion across the drift trajectories. It is the slowest degree of freedom, the nonadiabatic diffusion, that yields unbounded (extended) paths. Let us first consider the contribution to the velocity-velocity correlator (49) which comes from these extended trajectories, $\langle v_x(0)v_x(t)\rangle_{\rm ext}$. Following the approach developed in Sec. III, we parametrize it as a function of two variables

$$\langle v_x(0)v_x(t)\rangle_{\rm ext} = v_d^2 \frac{d}{\xi} F_\nu\left(\frac{v_d t}{d}, \frac{v_d t}{L}\right), \tag{50}$$

where $v_d=(3/8)^{1/2} v_F R_c B_0/d\overline{B}$ is the r.m.s. drift velocity, $\xi \propto R_d^{-\nu}$ and $L \propto R_d^{-\nu-1}$ are the characteristic size and perimeter of the elementary cell of the percolation network, and $\nu=4/3$. The factor d/ξ gives the partial density of the percolating states (i.e., the portion of the area $\xi\times\xi$ occupied by the trajectories of size ξ, $LR_d/\xi^2 \sim d/\xi$). At $d/v_d \ll t \ll L/v_d$, the scaling function exhibits a power-law behavior $F_\nu(\tau,0)\sim\tau^{-x}$ reflecting the fractal dimensionality of the links of the network. The exponent x can be found by equating $\langle v_x(0)v_x(t)\rangle_{\rm ext} t$ and the effective diffusion coefficient $\xi^2(t)/t$, where $\xi(t)\sim d[L(t)/d]^{\nu/(\nu+1)}$ and $L(t)\sim v_d t$, which yields $x=2/(\nu+1)=6/7$. The network model we have used is justified by the condition $x<1$ (the Harris criterion, $\nu>1$), so that the integral over t in Eq. (49) at $\omega=0$ is determined by $t\sim L/v_d$. We, thus, have

$$\langle v_x(0)v_x(t)\rangle_{\rm ext} \sim v_d^2 \frac{d}{\xi}\left(\frac{d}{v_d t}\right)^x, \quad \frac{d}{v_d} \lesssim t \lesssim \frac{L}{v_d}. \tag{51}$$

Now, to calculate the frequency-dependent correction to the *dc* conductivity at $\omega \lesssim v_d/L$, we need to know the behavior of the correlator (50) at $t \gg L/v_d$. If the diffusion over the percolation network were completely uncorrelated, F_ν would decay exponentially with increasing t. We will argue below that in fact F_ν falls off as a power law

$$F_\nu(\tau,\tau') \sim -(\tau'/\tau)^x/\tau'^2, \quad \tau \gg \tau' \gg 1.$$

For the correlator (50) this gives

$$\langle v_x(0)v_x(t)\rangle_{\rm ext} \sim -\frac{d\xi}{t^2}, \quad t \gtrsim \frac{L}{v_d}. \tag{52}$$

This long-time tail in the correlation function is similar to the one found in the Lorentz gas (noninteracting classical particles scattered by a random array of hard discs).[42] We will study the long-time correlations microscopically for the realistic case of a weak long-range disorder elsewhere;[32] here, we introduce a simple phenomenological model suitable for the qualitative description of the percolation network.

Consider the diffusion equation with an inhomogeneous diffusion coefficient $D(\mathbf{r})$. The diffusion current is then given by $D(\mathbf{r})\nabla n(\mathbf{r},t)$, where n is the concentration of particles. The diffusion propagator $n_{\omega\mathbf{q}}$ in $(\omega,\mathbf{q})$ space obeys the equation

$$-i\omega n_{\omega\mathbf{q}} + \int \frac{d^2\mathbf{q}'}{(2\pi)^2}(\mathbf{q}\mathbf{q}')D_{\mathbf{q}-\mathbf{q}'} n_{\omega\mathbf{q}'} = 1. \tag{53}$$

We now write $D(\mathbf{r})=D+\delta D(\mathbf{r})$, where D is the mean value of $D(\mathbf{r})$, expand the propagator in powers of δD, and average Eq. (53) over the fluctuations with the correlator $\langle \delta D(0)\delta D(\mathbf{r})\rangle = \Lambda D^2 g(r)$, where $g(r)$ is a dimensionless function of order unity, which falls off on the scale of d_0. The use of the diffusion equation implies that the correlation radius $d_0 \gg l$, where l is the mean-free path. To first order in Λ we have for the correction to the average diffusion propagator

$$\delta n_{\omega\mathbf{q}} = \Lambda D^2 \mathcal{D}_{\omega\mathbf{q}}^2 \int \frac{d^2\mathbf{q}'}{(2\pi)^2} g_{\mathbf{q}-\mathbf{q}'} (\mathbf{q}\mathbf{q}')^2 \mathcal{D}_{\omega\mathbf{q}'}, \tag{54}$$

where $\mathcal{D}_{\omega\mathbf{q}}=(-i\omega+Dq^2)^{-1}$. From Eq. (54) we deduce the ω dependent correction to the conductivity $\delta\sigma_{xx}(\omega) = e^2\rho\,\omega^2 \lim_{q\to 0} q^{-2}$ Re $\delta n_{\omega\mathbf{q}}$:

$$\frac{\delta\sigma_{xx}(\omega)}{\sigma_{xx}} = -\frac{\Lambda}{2}\int \frac{d^2\mathbf{q}}{(2\pi)^2} g_{\mathbf{q}} \frac{Dq^2}{-i\omega+Dq^2}, \tag{55}$$

i.e., $\delta\sigma_{xx}(\omega)/\sigma_{xx} \simeq \Lambda g_0 |\omega|/16D$ at small ω [we drop here an ω independent term in $\delta\sigma_{xx}(\omega)$], which implies a t^{-2} long-time tail in the velocity-velocity correlator in Eq. (49).

On the percolation network, the size of the effective scatterers and the effective mean free path are both of the order of ξ, i.e., $d_0 \sim l \sim \xi$. Furthermore, strong fluctuations of the geometry of the percolating cluster imply that $\Lambda \sim 1$. We expect that the $1/t^2$ tail, the existence of which has been demonstrated above in the phenomenological model with $d_0 \gg l$ and $\Lambda \ll 1$, will not disappear if we set $d_0 \sim l$ and $\Lambda \sim 1$. Substituting these estimates into Eq. (55) we get

$$\frac{\delta\sigma_{xx}(\omega)}{\sigma_{xx}} \sim \frac{|\omega|L}{v_d}, \quad |\omega| \lesssim \frac{v_d}{L}, \tag{56}$$

which corresponds to Eq. (52).[43] We recall that the characteristic scale L entering Eq. (56) is given by

$$L \sim d\left[\frac{me^2 v_d d}{\sigma_{xx}\hbar^2}\right]^{7/3} \propto d\exp\left(\frac{7}{13}S_{\rm min}\right). \tag{57}$$

It is worth noting that the *classical* kinetic correlations compete with the quantum ones and win, unless the frequency is exponentially small. Specifically, as is well known, the quantum localization effects in 2D lead to a t^{-1} tail in the correlator (49) and, correspondingly, to a $\ln|\omega|$ correction to the conductivity. This quantum correction is of special interest because of its divergence for $\omega\to 0$, in the thermodynamic limit. The classical correction, proportional to $|\omega|$, does not diverge, but it is also interesting, both theoretically and experimentally, since it is *nonanalytical* in ω and is much larger than the quantum one even at very low ω. The point is that the localization correction is a series in powers of the small parameter $1/k_F l$, where k_F is the Fermi wave vector, while the relevant parameter for the classical corrections is d/l, where d is the correlation radius of disorder. If the disorder is long-ranged ($k_F d \gg 1$), the classical correc-

tions are dominant in a wide range of ω. We will discuss the classical corrections in more detail elsewhere.[32]

Note that $\sigma_{xx}(\omega)$ behaves nonanalytically at half-filling also in the *integer* quantum Hall regime. At the integer quantum Hall transition, the frequency-dependent correction $\delta\sigma_{xx}\sim|\omega|^{y/2}$ is related to corrections to scaling. The leading irrelevant scaling exponent y at the quantum phase transition was found numerically to be equal to 0.38 ± 0.04 and 0.35 ± 0.05 in Refs. 44 and 45, respectively. In Ref. 46, y was argued to be equal to η, where $\eta\simeq0.4$ (Refs. 47,44) is the critical exponent of eigenfunction correlations. However, in a long-range random potential there exists a classical nonanalytic term $\delta\sigma_{xx}\sim|\omega|^{y_{\rm cl}/2}$ with $y_{\rm cl}\simeq2$,[48] which dominates $\delta\sigma_{xx}(\omega)$ in a wide range of frequencies.

Coming back to Eq. (56), we see that the frequency-dependent correction becomes strong at $\omega\sim v_d/L$. We now turn to higher frequencies. The scaling form (51) implies that the contribution to $\sigma_{xx}(\omega)$ from the extended trajectories behaves as ω^{-1+x} at $\omega\gg v_d/L$, i.e., it slowly decreases as $\omega^{-1/7}$ with increasing frequency. Let us show that the extended trajectories do not determine the conductivity any more and the main contribution to $\sigma_{xx}(\omega)$ comes now from localized drift trajectories. We will show that in fact $\sigma_{xx}(\omega)$ *grows* with ω. We neglect the weak nonadiabatic scattering between the closed drift trajectories and represent the velocity-velocity correlator (49) for the periodic drift orbits in the form

$$\langle|v_x|^2_\omega\rangle_{\rm loc}=\pi\omega^2\left\langle\left|\int_0^T\frac{dt}{T}x(t)e^{i\omega t}\right|^2\sum_n\ \delta\left(\omega-\frac{2\pi n}{T}\right)\right\rangle. \tag{58}$$

Here, $\mathbf{r}(t)$ is a closed trajectory with the period T and the angular brackets denote the average over both T and the shape of the trajectory at given T. The average is determined by trajectories with $T\sim\omega^{-1}$, their perimeter and size are $L_\omega\sim v_d/\omega$ and $\xi_\omega\sim d(L_\omega/d)^{\nu/(\nu+1)}$, respectively. The partial density of states corresponding to these trajectories is $\sim\rho_{Fd/\xi_\omega}$ [see the paragraph after Eq. (50)]. The estimate for the correlator (58) thus reads

$$\langle|v_x|^2_\omega\rangle_{\rm loc}\sim\omega^2\xi_\omega^2\times d/\xi_\omega\times|\omega|^{-1}, \tag{59}$$

where the factor d/ξ_ω stands for the partial density of states and the last factor ω^{-1} comes from the averaging of the delta functions in Eq. (58). This yields the *ac* conductivity of the form

$$\sigma_{xx}(\omega)\sim e^2\rho_F v_d R_\omega, \tag{60}$$

where $R_\omega\sim d(d/\xi_\omega)^{1/\nu}\propto|\omega|^{3/7}$ is the characteristic width of the links of the conducting network. We get[49]

$$\sigma_{xx}(\omega)\sim\sigma_{xx}(0)\left(\frac{|\omega|L}{v_d}\right)^{3/7},\quad \frac{v_d}{L}\lesssim|\omega|\lesssim\frac{v_d}{d}. \tag{61}$$

Equations (56) and (61) describe the behavior of the conductivity at $\omega\lesssim v_d/d$. At still higher frequencies, $\sigma_{xx}(\omega)$ is determined by the velocity-velocity correlations in the crossover region between the ''ballistic'' drift on the spatial scale much smaller than d and the ''diffusive'' motion over the fractal network on larger scales. At the crossover, the velocity-velocity correlator can be parametrized as $\langle v_x(0)v_x(t)\rangle=v_d^2f_v(v_dt/d)$, where $f_v(\tau)$ is a dimensionless function of order unity [cf. Eq. (50)]. Note that it is not sufficient at $\omega\gg v_d/d$ to know the behavior of the correlator at $t\sim\omega^{-1}$. Since the conductivity is expressed in terms of the high-frequency Fourier component of $\langle v_x(0)v_x(t)\rangle$, which is an even function of t, σ_{xx} will fall off exponentially with increasing ω (until ω reaches the low-frequency wing of the cyclotron resonance). Therefore, to get the asymptotic behavior of $\sigma_{xx}(\omega)$, we need to know the analytical properties of the correlator as a function of t, i.e., the exact shape of the function $f_v(\tau)$, which requires a numerical simulation. We expect, however, that the function $f_v(\tau)$ has a simple analytical structure with singular points at Im $\tau\sim\pm1$, which yields the exponential falloff of the form

$$\ln\sigma_{xx}\sim-|\omega|d/v_d. \tag{62}$$

This exponential decay of σ_{xx} is limited from the side of large frequencies by the disorder-broadened cyclotron resonance, which dominates $\sigma_{xx}(\omega)$ at $\omega\sim\omega_c=e\overline{B}/mc$.

The arguments of the last paragraph concerning the exponential falloff at large ω are also applicable to the *ac* conductivity in zero (or low) $\overline{B}$, with the only substitution of the Fermi velocity v_F for the drift velocity v_d. In contrast to the Drude (white-noise disorder) case, where the velocity-velocity correlation function has a cusp at $t=0$ leading to the slow $1/\omega^2$ decrease of $\sigma_{xx}(\omega)$, in the case of smooth disorder $\langle v_x(0)v_x(t)\rangle$ is an analytic function of t at $t=0$, which implies an exponential decay of $\sigma_{xx}(\omega)$ at $\omega\gg v_F/d$.

Figure 11 shows the results of the numerical calculation of the *ac* conductivity for $\alpha=0.35$. Significant deviations from the Drude theory fit are seen, which become stronger with increasing external magnetic field $\overline{B}$. For zero (or low) $\overline{B}$ the results are still relatively close to the Drude theory, except in the tail (for $\omega\gg v_F/d$), where the conductivity starts to drop exponentially (see inset), in qualitative agreement with the theoretical expectation [Eq. (62)]. In the intermediate fields $\overline{B}$ (see the curves corresponding to $\omega_cd/v_F=0.2$ and 0.37) the nonanalytic dip (56) around $\omega=0$ gets clearly observed. Finally, in a large magnetic field, the shape of the *ac* conductivity is completely different: it increases nonanalytically at small ω in agreement with Eq. (61), see Fig. 12, and then drops exponentially in a higher frequency range in agreement with Eq. (62), see Fig. 13; at still higher frequencies, the cyclotron resonance (smeared by disorder) is observed. It becomes difficult to resolve reliably the leading nonanalytic correction $\delta\sigma_{xx}\propto|\omega|$ at $\omega\to0$ in high magnetic fields, since it is shifted to the very low ω range and is masked by the statistical noise present in the numerical data. Note that in Figs. 12 and 13 we used the frequency scale v_d/d, which is a natural scale in the regime of high-magnetic field. The value of α in Fig. 11 is approximately the one appropriate for the CF system. Therefore, this figure represents our prediction for the *ac* conductivity of the CF's at half filling ($\overline{B}=0$) and away from it ($\overline{B}\neq0$).

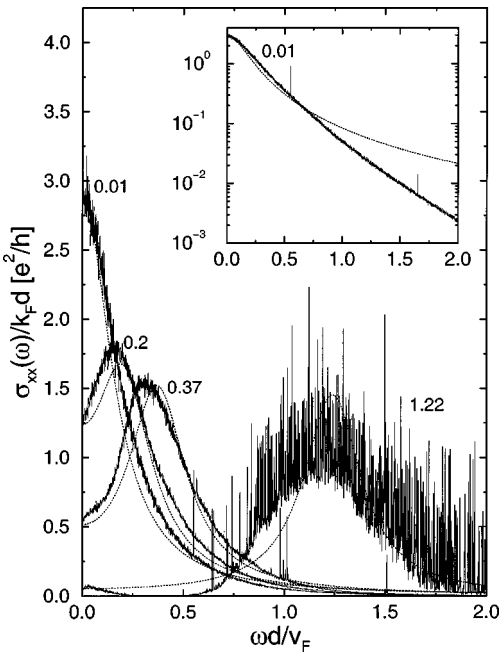

FIG. 11. ac conductivity at $\alpha=0.35$ and for different values of the magnetic field $\bar{B}$. The number near each curve indicates the value of the cyclotron frequency $\omega_c=e\bar{B}/mc$ in units of v_F/d; to convert these values into $\bar{B}/B_0$, one has to multiply them by $1/\alpha$. The result of Drude theory is also shown (dotted lines). The statistical noise in the data at $\omega_c d/v_F=1.22$ is due to fluctuations of the local cyclotron frequency. Inset: the low-$\bar{B}$ data ($\omega_c d/v_F=0.01$) on a logarithmic scale.

B. ac conductivity at $\alpha \gg 1$, $\bar{B}=0$

Let us now consider the frequency dispersion of the snake-state percolation ($\alpha \gg 1$, $\bar{B}=0$). Since the mechanism of the percolation was of no importance in the derivation of Eq. (56), we get

$$\frac{\delta\sigma_{xx}(\omega)}{\sigma_{xx}} \sim \frac{|\omega| L_s}{v_F}, \quad |\omega| \lesssim \frac{v_F}{L_s} \tag{63}$$

(we substituted here v_F for v_d as the effective drift velocity of the snake states and $L_s \sim d\alpha^{14/9}$ for the perimeter of the elementary cell of the conducting network). The correction becomes strong at $|\omega| \sim v_F/L_s$. At larger ω, the conductivity is determined by the snake states that are bounded to the closed zero-B contours of size much smaller than ξ_s. Specifically, the main contribution to $\sigma_{xx}(\omega)$ now comes from the trajectories of the length $L_\omega \sim v_F/\omega$. We estimate their contribution at $|\omega| \gtrsim v_F/L_s$ as

$$\sigma_{xx}(\omega) \sim e^2 \frac{\rho R_s L_\omega \theta_s^2}{\xi_\omega^2} \xi_\omega^2 \omega \sim \sigma_{xx}(0), \tag{64}$$

$$\frac{v_F}{L_s} \lesssim |\omega| \lesssim \frac{v_F \rho_s}{d^2},$$

where $\xi_\omega \sim d(L_\omega/d)^{\nu/(\nu+1)}$. The first factor gives the density of states for the snake-state orbits with the periods larger than ω^{-1}, while the last factor is the effective diffusion coefficient on the time scale of order ω^{-1}. We see that ω cancels out in this expression and $\sigma_{xx}(\omega)$ turns out to be of order $\sigma_{xx}(0)$ [Eq. (16)]. We put $|\omega| \sim v_F \rho_s/d^2 \sim v_F/d\alpha^{2/3}$ as the upper limit for the frequency range where Eq. (64) is valid: strictly speaking, the decrease of L_ω at higher $|\omega|$ is accompanied with a growth of the phase volume of the snake states that participate in the *ac* transport by escaping the adiabatic traps. This means that the angle θ which should be substituted for θ_s, Eq. (13), now increases with $|\omega|$ as $\mathcal{L}_\omega^{-1/2}$, where $\mathcal{L}_\omega \sim \ln^{1/4}(v_F/|\omega| d)$. It follows that

$$\sigma_{xx}(\omega) \sim \sigma_{xx}(0) \frac{\mathcal{L}}{\mathcal{L}_\omega}, \quad \frac{v_F \rho_s}{d^2} \lesssim |\omega| \lesssim \frac{v_F}{d}, \tag{65}$$

i.e., the conductivity grows with increasing ω (but extremely slowly), until $|\omega|$ becomes of the order of v_F/d.

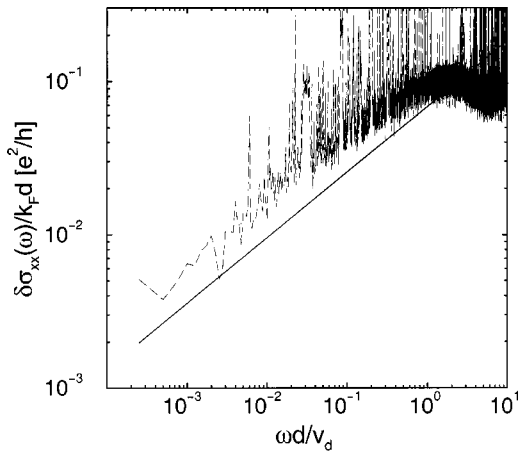

FIG. 12. Low-frequency behavior of the ac conductivity $\delta\sigma_{xx}(\omega)=\sigma_{xx}(\omega)-\sigma_{xx}(0)$ in strong magnetic field for $\alpha=4.04$, $\bar{B}/B_0=1.00$ (which corresponds to $\omega_c d/v_F=4.04$). The straight line corresponds to the theoretical prediction $\delta\sigma_{xx} \propto |\omega|^{3/7}$, see Eq. (61). The same nonanalytic behavior of $\sigma_{xx}(\omega)$ in the low-ω range in strong magnetic field $\bar{B}$ takes place for small α and is in particular seen in Fig. 13 for $\alpha=0.2$.

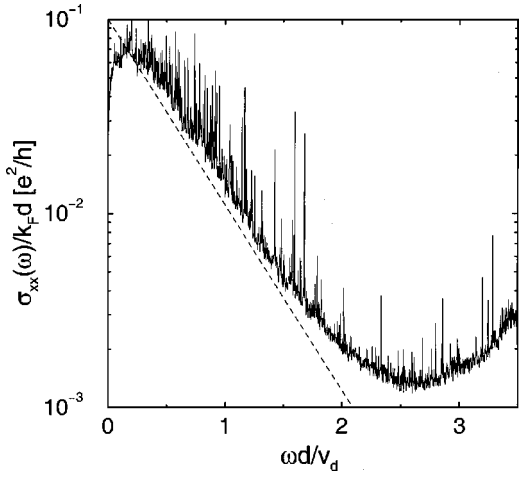

FIG. 13. ac conductivity at $\alpha=0.2$ and strong magnetic field, $\bar{B}/B_0=4.38$ (which corresponds to $\omega_c d/v_F=0.88$), shows the exponential falloff (62) in the intermediate range of frequencies. The dotted line corresponds to $\ln \sigma_{xx} = -2.2|\omega| d/v_d$.

Note that, in the derivation of Eqs. (64) and (65), we restricted ourselves to the snake states and were not concerned about the contribution of the drift trajectories, which requires comment. Indeed, one might think that the arguments that led to the power-law behavior of $\sigma_{xx}(\omega)$ in Eq. (61) could be used here as well. However, there is a new feature that makes the percolation at large α and zero $\overline{B}$ distinct from that at $\alpha\sim 1$ and large $\overline{B}$. Namely, now there is no characteristic drift velocity v_d, which is the same for all trajectories. Specifically, v_d at large α depends on the typical distance $\mathcal{R}$ between the drift trajectory and the zero-B contour. We parametrize $v_d(\mathcal{R})$ as

$$v_d(\mathcal{R}) = v_F F_s\left(\frac{\mathcal{R}}{R_s}\right), \tag{66}$$

where $F_s(0)\sim 1$ and $F_s(x)\sim -x^{-2}$ at $x\gg 1$. The slowing down of the drift with increasing $\mathcal{R}$ is related to the linear growth of the magnetic field as one moves away from the line $B=0$. Equation (60) tells us that the contribution to the *ac* conductivity of trajectories separated by the distance $\mathcal{R}$ from the zero-δB lines scales as $v_d(\mathcal{R})\mathcal{R}\propto\mathcal{R}^{-1}$, i.e., it *decreases* with $\mathcal{R}$. It follows that the drift orbits that surround the snake-state trajectories do not contribute to $\sigma_{xx}(\omega)$ even at large ω.[50]

Thus, the overall picture in the snake-state percolation regime is as follows: $\sigma_{xx}(\omega)$ exhibits a narrow dip around $\omega=0$, increasing linearly with growing ω; this increase is saturated at $\omega\sim v_F/L_s$ where the ω-dependent correction becomes strong; finally, on the (parametrically larger) scale of $\omega\sim v_F/d$, $\sigma_{xx}(\omega)$ starts to fall off exponentially.[51] The latter regime is similar to that at large $\overline{B}$ [see the paragraph after Eq. (61)].

We finally comment on the case $\alpha\sim 1$, $\overline{B}=0$ relevant to the CF problem. In this case $L_s\sim d$, so that the range of applicability of Eqs. (64) and (65) shrinks away and the *ac* conductivity becomes a function of the single variable $\omega d/v_F$:

$$\sigma_{xx}(\omega)\sim\sigma_{xx}(0)F_\omega\left(\frac{\omega d}{v_F}\right), \tag{67}$$

where $F_\omega(x)-F_\omega(0)\sim|x|$ at $|x|\lesssim 1$ and $F_\omega(x)$ falls off exponentially at larger x ($\ln F_\omega\sim-|x|$). We have already discussed the exponential behavior at large ω in the considered regime $\alpha\sim 1$, $\overline{B}=0$ in the end of Sec. IV A; it is clearly seen in Figs. 11 and 14. As to the nonanalytic dip at small ω, our numerical simulations indicate that it is almost unobservable at the values of α describing the CF conductivity ($\alpha\lesssim 0.7$) at $\overline{B}=0$. Apparently, the corresponding numerical coefficient gets very small for such values of α. With increasing either α (Fig. 14) or $\overline{B}$ (Fig. 11) the nonanalytic structure gets resolved very clearly.

In Fig. 14, we show the *ac* conductivity at relatively large $\alpha=4.04$ in comparison with that at $\alpha=0.5$. The $\alpha=4.04$ curve is strikingly different from the Drude behavior and shows the features discussed above: the nonanalytic increase in the small ω region, followed by a rapid decay consistent with the theoretically predicted exponential falloff. At still higher frequencies a broad distribution of cyclotron resonances in the local (random) magnetic field is observed. A hump at $\omega d/v_F\simeq 1.7$ marks the onset of this regime and corresponds to the characteristic snake state frequency $\omega\sim\alpha^{1/2}(v_F/d)$. To see the exponential falloff in a broader frequency range more clearly, one would have to consider larger values of α.

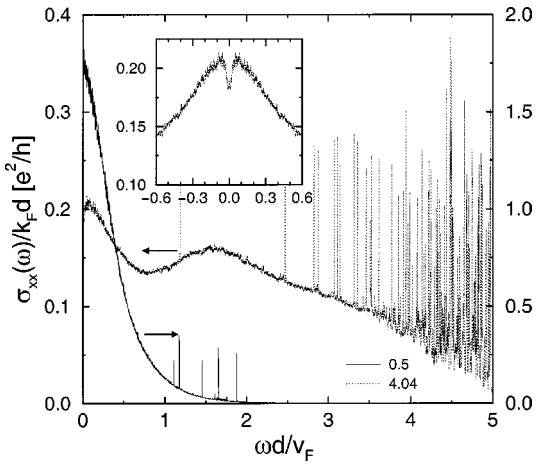

FIG. 14. ac conductivity in zero $\overline{B}$ at $\alpha=0.5$ and $\alpha=4.04$. The scaling of the y axis is different for the two curves, as indicated by the arrows. Inset: nonanalytic dip around $\omega=0$ [Eq. (63)] at $\alpha=4.04$.

V. CONCLUSIONS

We have presented a detailed analytical and numerical study of the conductivity of a 2D fermion gas in a smooth random magnetic field, in the whole range of the parameters α (strength of the random field), $\overline{B}$ (mean magnetic field), and ω (frequency). While special emphasis has been put on the application of our results to the composite-fermion description of the half-filled Landau level, they may be equally relevant to the electron transport in a real random magnetic field. Below, we summarize the main findings.

(1) At zero magnetic field $\overline{B}$, the *dc* transport has a totally different character in the regimes of weak ($\alpha\ll 1$) and strong ($\alpha\gg 1$) disorder. While in the former case $\sigma_{xx}\propto 1/\alpha^2$ [Eq. (2)] is correctly given by the Born approximation, in the latter the conductivity is determined by the percolation of snake states yielding $\sigma_{xx}\propto 1/\alpha^{1/2}$ (up to a negligibly weak logarithmic correction), see Eq. (16). Numerical simulations confirm these analytical findings and allow us to find σ_{xx} in the crossover region $\alpha\sim 1$, see Fig. 7.

(2) In strong mean magnetic field $\overline{B}$ the particle motion takes the form of an adiabatic drift of the cyclotron orbits. A nonzero value of σ_{xx} in this regime is entirely due to exponentially weak nonadiabatic scattering processes. As a consequence, the conductivity falls off exponentially, $-\ln\sigma_{xx}\propto\overline{B}^2$, see Eqs. (27), (35), and (36). [At $\alpha\ll 1$, an intermediate regime appears, $-\ln\sigma_{xx}\propto\overline{B}$, see Eq. (40).] The numerical simulations have allowed us to find the shape of the magnetoresistance in a wide range of $\overline{B}$ for the values of α ranging from 0.2 to 5, see Fig. 9. The magnetoresistance $\rho_{xx}(\overline{B})$

shows a sharp falloff at large $\overline{B}$ in agreement with the analytical results. Furthermore, at $\alpha \lesssim 0.5$ this falloff is preceded by a positive magnetoresistance in the intermediate range of $\overline{B}$. The whole shape of $\rho_{xx}(\overline{B})$ at $\alpha \sim 0.35$ (as well as its absolute value) is surprisingly similar to the experimental magnetoresistivity in the fractional quantum Hall effect around $\nu = 1/2$ (Fig. 8).

(3) In contrast to the case of a short-range random potential, the quantum magnetooscillations of the conductivity start to develop in the range of the magnetic field $\overline{B}$ where the dimensionless conductivity $g = \sigma_{xx}/(e^2/h)$ drops to a value ~ 1, in agreement with experiment (Fig. 10). These oscillations are not related to those of the total density of states (which are damped much more strongly), but are determined by the oscillations of the density of states of the particles moving on the percolating network, as well as by the quantum localization effects.

(4) The ac conductivity also shows distinct features related to the deviations of the particle kinetics from the behavior following from the Boltzmann equation. While at $\alpha \ll 1$ and $\overline{B} = 0$ the *ac* conductivity $\sigma_{xx}(\omega)$ is relatively close to the Drude form (except in the tail, where it drops exponentially), at large α and/or $\overline{B}$ the shape of $\sigma_{xx}(\omega)$ becomes totally different. Specifically, it shows nonanalytic behavior in the low-frequency range, see Eqs. (56), (61), and (63) and Figs. 11–14, related to the long-time tails in the velocity-velocity correlation function and reflecting the strongly non-Boltzmann character of the transport in the percolating regime. At higher frequencies, $\sigma_{xx}(\omega)$ starts to drop exponentially (which reflects the ''ballistic'' dynamics of the snake states or drifting orbits on short spatial scales), until it reaches the low-frequency wing of the disorder-broadened cyclotron resonance peak, see Eq. (62) and Fig. 13. The *ac* conductivity at $\alpha = 0.35$ (which is in the range of α relevant to the composite-fermion problem) and different values of the mean magnetic field $\overline{B}$ shown in Fig. 11 clearly demonstrates the anomalies which we expect to be observed in the *ac* transport around $\nu = 1/2$.

ACKNOWLEDGMENTS

We are grateful to P.T. Coleridge, J.H. Smet, H.L. Stormer, and A.S. Yeh for sending us the experimental data used in Figs. 8 and 10, and for valuable comments concerning the details of the experiments. We thank J. Wilke for the help in the numerical simulations of the snake-state dynamics. This work was supported by the SFB195 and the Graduiertenkolleg ''Kollektive Phänomene im Festkörper'' der Deutschen Forschungsgemeinschaft, and by INTAS Grant No. 97-1342 and RFBR Grant No. 99-02-17093.

*Also at Petersburg Nuclear Physics Institute, 188350 St. Petersburg, Russia.

†Also at A.F. Ioffe Physico-Technical Institute, 194021 St. Petersburg, Russia.

[1] J.K. Jain, Phys. Rev. Lett. **63**, 199 (1989); in *Perspectives in Quantum Hall Effects: Novel Quantum Liquids in Low-Dimensional Semiconductor Structures*, edited by S. Das Sarma and A. Pinczuk (Wiley, New York, 1997), p. 265.

[2] B.I. Halperin, P.A. Lee, and N. Read, Phys. Rev. B **47**, 7312 (1993).

[3] See the reviews: H.L. Stormer and D.C. Tsui, in *Perspectives in Quantum Hall Effects: Novel Quantum Liquids in Low-Dimensional Semiconductor Structures* (Ref. 1) p. 385; R.L. Willett, Adv. Phys. **46**, 447 (1997); J.H. Smet, in *Composite Fermions*, edited by O. Heinonen (World Scientific, Singapore, 1998), p. 443, and references therein.

[4] S.J. Bending, K. von Klitzing, and K. Ploog, Phys. Rev. Lett. **65**, 1060 (1990).

[5] A. Geim, S. Bending, and I. Grigorieva, Phys. Rev. Lett. **69**, 2252 (1992); A. Geim, S. Bending, I. Grigorieva, and M.G. Blamire, Phys. Rev. B **49**, 5749 (1994).

[6] P.D. Ye, D. Weiss, G. Lütjering, R.R. Gerhardts, K. von Klitzing, K. Eberl, H. Nickel, and G. Weimann, in *Proceedings of the 23rd International Conference on The Physics of Semiconductors*, edited by M. Scheffler and R. Zimmermann (World Scientific, Singapore, 1996), p. 1529.

[7] F.B. Mancoff, R.M. Clarke, C.M. Marcus, S.C. Zhang, K. Campman, and A.C. Gossard, Phys. Rev. B **51**, 13 269 (1995); L. Zielinski, K. Chaltikian, K. Birnbaum, C.M. Marcus, K. Campman, and A.C. Gossard, Europhys. Lett. **42**, 73 (1998).

[8] A.G. Aronov, A.D. Mirlin, and P. Wölfle, Phys. Rev. B **49**, 16 609 (1994).

[9] Y.B. Kim, A. Furusaki, and D.K.K. Lee, Phys. Rev. B **52**, 16 646 (1995).

[10] A. Furusaki, Phys. Rev. Lett. **82**, 604 (1999). Note that within the lattice random flux model the localization length diverges in the center of the band, because of an additional symmetry at this point. This is, however, irrelevant to the continuum model, where all states are localized.

[11] A. Smith, R. Taboryski, L.T. Hansen, C.B. Sorensen, P. Hedegard, and P.E. Lindelof, Phys. Rev. B **50**, 14 726 (1994); P. Hedegard and A. Smith, *ibid.* **51**, 10 869 (1995).

[12] D.B. Chklovskii and P.A. Lee, Phys. Rev. B **48**, 18 060 (1993); D.B. Chklovskii, *ibid.* **51**, 9895 (1995). The quantum-mechanical treatment of the snake states in a constant-gradient field can be found in J.E. Müller, Phys. Rev. Lett. **68**, 385 (1992).

[13] D.K.K. Lee, J.T. Chalker, and D.Y.K. Ko, Phys. Rev. B **50**, 5272 (1994).

[14] M.M. Fogler, A.Yu. Dobin, V.I. Perel, and B.I. Shklovskii, Phys. Rev. B **56**, 6823 (1997).

[15] G.M. Zaslavsky, R.Z. Sagdeev, D.A. Usikov, and A.A. Chernikov, *Weak Chaos and Quasi Regular Patterns* (Cambridge University, Cambridge, 1991).

[16] A.D. Mirlin, D.G. Polyakov, and P. Wölfle, Phys. Rev. Lett. **80**, 2429 (1998).

[17] A.G. Aronov, E. Altshuler, A.D. Mirlin, and P. Wölfle, Phys. Rev. B **52**, 4708 (1995); A.D. Mirlin, E. Altshuler, and P. Wölfle, Ann. Phys. (Leipzig) **5**, 281 (1996).

[18] M.B. Isichenko, Rev. Mod. Phys. **64**, 961 (1992).

[19] The logarithmic factor $\mathcal{L}$ was omitted in Ref. 16.

[20] D.V. Khveshchenko, Phys. Rev. Lett. **77**, 1817 (1996).

[21] E. Buks, M. Heiblum, Y. Levinson, and H. Shtrikman, Semicond. Sci. Technol. **9**, 2031 (1994).

[22] P.T. Coleridge, Phys. Rev. B **44**, 3793 (1991).
[23] A. Stern and B.I. Halperin, Phys. Rev. B **52**, 5890 (1995); R. Shankar and G. Murthy, Phys. Rev. Lett. **79**, 4437 (1997); S.H. Simon, in *Composite Fermions* (Ref. 3), p. 91.
[24] R.R. Du, H.L. Stormer, D.C. Tsui, A.S. Yeh, L.N. Pfeiffer, and K.W. West, Phys. Rev. Lett. **73**, 3274 (1994).
[25] P.T. Coleridge, Z.W. Wasilewski, P. Zawadzki, A.S. Sachrajda, and H.A. Carmona, Phys. Rev. B **52**, 11 603 (1995).
[26] D.V. Khveshchenko, Phys. Rev. Lett. **77**, 362 (1996); A.D. Mirlin and P. Wölfle, Phys. Rev. B **55**, 5141 (1997).
[27] F. Evers, A.D. Mirlin, D.G. Polyakov, and P. Wölfle, Phys. Rev. B **58**, 15 321 (1998).
[28] Note that, for the purpose of the calculation of $S_{\min}$, the integration in Eq. (29) along the axis of Ims can be done within any interval of the form $(-id+ia, id+ia)$ with arbitrary a. The choice $a=0$ corresponds to the condition that the optimum fluctuation $v_d^0(s)$ is real on the real axis of s.
[29] It is worthwhile to notice that the exponential falloff of σ_{xx} with increasing $\overline{B}$ is limited by inelastic scattering and by scattering on short-range static inhomogeneities—these scattering processes allow an electron to change drift trajectories and thus provide a mechanism of percolation competing with the nonadiabatic transitions (Refs. 18 and 7).
[30] J.H. Smet and V. Umansky (unpublished).
[31] A.S. Yeh, R.R. Du, H.L. Stormer, D.C. Tsui, L.N. Pfeiffer, K.W. Baldwin, and K.W. West (unpublished).
[32] A. D. Mirlin, J. Wilke, F. Evers, D. G. Polyakov, and P. Wölfle, Phys. Rev. Lett. (to be published); J. Wilke, A. D. Mirlin, D. G. Polyakov, F. Evers, and P. Wölfle (unpublished).
[33] T. Ando, J. Phys. Soc. Jpn. **37**, 1233 (1974).
[34] A. Isihara, *Electron Liquids* (Springer, New York, 1993).
[35] D. Shoenberg, *Magnetic Oscillations in Metals* (Cambridge University, Cambridge, 1984).
[36] P. Coleridge, R. Stoner, and R. Fletcher, Phys. Rev. B **39**, 1120 (1989).
[37] M.E. Raikh and T.V. Shahbazyan, Phys. Rev. B **47**, 1522 (1993).
[38] B. Laikhtman and E.L. Altshuler, Ann. Phys. (N.Y.) **232**, 332 (1994).
[39] K. Richter, Europhys. Lett. **29**, 7 (1995).
[40] G. Hackenbroich and F. von Oppen, Europhys. Lett. **29**, 151 (1995).
[41] A.M.M. Pruisken, in *The Quantum Hall Effect*, edited by R.E. Prange and S.M. Girvin (Springer, Berlin, 1987), p. 117.
[42] M.H. Ernst and A. Weyland, Phys. Lett. **34A**, 39 (1971); E.H. Hauge, in *Transport Phenomena*, edited by G. Kirczenow and J. Marro, Lecture Notes in Physics Vol. 31 (Springer, Berlin, 1974), p. 337.
[43] Though for the model that we consider here the sign of the tail in the velocity-velocity correlator is negative, $\delta\sigma_{xx}(\omega) \propto +|\omega|$, the sign depends on the type of disorder (Ref. 32).
[44] B. Huckestein, Rev. Mod. Phys. **67**, 357 (1995).
[45] F. Evers and W. Brenig, Phys. Rev. B **57**, 1805 (1998).
[46] D.G. Polyakov, Phys. Rev. Lett. **81**, 4696 (1998).
[47] J.T. Chalker and G.J. Daniell, Phys. Rev. Lett. **61**, 593 (1988).
[48] F. Evers and W. Brenig, Z. Phys. B **94**, 155 (1994).
[49] Let us note that a similar in spirit consideration was presented in the essentially different context of the surface acoustic wave absorption around $\nu=1/2$ in the integer quantum Hall regime, in A. Knäbchen, Y.B. Levinson, and O. Entin-Wohlman, Phys. Rev. B **54**, 10 696 (1996). There, σ_{xx} at half-filling is almost independent of ω, in contrast to Eq. (61), but the width $\Delta\nu$ of the absorption peak behaves in a similar fashion: $\Delta\nu \sim R_\omega/d \propto |\omega|^{3/7}$.
[50] In fact, we should consider here only the drift trajectories with $\mathcal{R} \gtrsim \mathcal{R}_c = R_s(\ln\alpha)^{1/4}$, which are decoupled from the snake states. The drift orbits with smaller $\mathcal{R}$ transform into the snake states with $\theta \sim 1$ and so are localized by the adiabatic ''mirrors,'' as discussed in Sec. II. The estimate for $\mathcal{R}_c$ can be obtained by calculating the probability for a drifting cyclotron orbit to hit a region with an anomalously large gradient of $B(\mathbf{r})$, which is necessary for the adiabatic transformation of the orbit into a snake state.
[51] The extremely slow growth (65) in the intermediate range of ω is hardly observable for any realistic α.